ALTERNATIVE FUEL ENGINE CONTROL SYSTEM

by

YUAN ZHU, B.S.E.

A THESIS

IN

ELECTRICAL ENGINEERING

Submitted to the Graduate Faculty
of Texas Tech University in
Partial Fulfillment of
the Requirements for
the Degree of

MASTER OF SCIENCE

IN

ELECTRICAL ENGINEERING

Approved

December, 1997

ACKNOWLEDGEMENTS

My sincere thanks goes to my thesis advisor, Dr. Micheal E. Parten, for his valuable guidance and morale support throughout this research. Appreciation is also extended to Dr. Donald C. Wunsch and Dr. Timothy T. Maxwell for their valuable comments and serving on my thesis committee.

I would like to thank all of the members of the 1996 and 1997 Texas Tech Propane Minivan teams.

A special thank is expressed to my parents for their patience and encouragement during my pursuit of a graduate degree.

TABLE OF CONTENTS

LIST OF TABLES

LIST OF FIGURES

CHAPTER 1

INTRODUCTION

As air quality decreases in urban areas across the United States, state and national regulatory agencies are passing more stringent automobile emission standards. In addition, the need for alternative methods of transportation is growing as the United States' dependency on foreign oil increases from year to year [1]. While new technologies are constantly introduced to improve emission and fuel economy on conventional gasoline vehicles, alternative fuel technology has emerged as a more promising solution.

California is the pioneer in setting stringent automobile emission standards. The California Air Resources Board (CARB) has developed a four-tier low emission vehicle standard that includes a transitional low emission vehicle (TLEV), a low emission vehicle (LEV), an ultra-low emission vehicle (ULEV), and a zero emission vehicle (ZEV). The emission levels required under these standards are included in Table 1 1 The standards require that LEV standard go into effect in 1997 for 25% of the vehicles sold in California while another two percent meet ULEV emission standard. Beginning in 1998, two percent of cars sold in the state must have zero tail-pipe emission. Thirteen northeastern states have adopted California's LEV standards, and new federal emission standards, patterned after tough California standards, were introduced in 1996 [2].

As domestic petroleum resources become depleted, the U.S. depends more and more on foreign oil. Currently half of this country's crude oil (and automotive fuel) needs are satisfied by import [2]. Some states have realized this situation and taken action or are

taking action against automobiles that have poor fuel economy Fuel economy is a major issue with consumers as well as regulatory agencies.

Table 1.1 California Emission Standards (g mile): 50,000 Mile Standards (100,000 Mile Standards)

Standard	Nonmethane Organic Gases (NMOG)	Carbon Monoxide (CO)	Nitrogen Oxides (NOx)
Transitional low emissions vehicle (TLEV)	0.125 (0.156)	3.4 (4.2)	0.20 (0.60)
Low emissions vehicle (LEV)	0.0750 (0.090)	3.4 (4.2)	0.20 (0.30)
Ultra-low emissions vehicles (ULEV)	0.040 (0.055)	1.7 (2.1)	0.20 (0.30)
Zero emissions vehicles (ZEV)	0.00 (0.00)	0.0 (0.0)	0.00 (0.00)

Alternative fuels are fuels that can be derived from non-crude oil resources Among the popular alternative fuels are natural gas, propane, methanol, ethanol and hydrogen. Alternative fuels provide three distinct advantages over gasoline and diesel fuels. First, alternative fuels can be produced largely, if not totally, from domestic resources and thus significantly reduce the nation's dependence on imported crude oil. Second, having much simpler and smaller molecules, alternative fuels are potentially capable of lowering vehicular emissions. Third, alternative fuels have the potential of reducing vehicle operation cost [2].

Over the past few years, Texas Tech has been actively involved in alternative fuel research. Students from the College of Engineering at Texas Tech have successfully participated in numerous student alternative fuel vehicle competitions In these competitions, conventional gasoline vehicles were converted to run on some kind of

alternative fuel [21]. The engine controllers used in these converted vehicles are in· gasoline controllers or some type of universal after-market conversion controller. There are aspects of engine control that are fuel or engine-specific and have to be optimized for the specific fuel or engine. Among these aspects are most open-loop controls using static lookup tables, e.g., spark advance control and cold-start enrichment control. Since control parameters are not accessible in commercial engine controllers, optimization of the conversion using a non-dedicated engine controller is often impossible. In many cases, the advantages of alternative fuels are significantly reduced as compared to conventional gasoline fuel, because of the inadequacy of the controller. To have a candid evaluation of the alternative fuel's potential as an automobile fuel, the conversion system has to be fully optimized for that specific fuel and engine. This calls for an engine controller that is known to us and easy to modify. This leads to the desired long-range goal of this research to develop a configurable engine controller.

Microprocessor-based engine controllers were first introduced in 1977 in the GM Oldsmobile [4]. Since then, tremendous advances have been made in engine control technology. Embedded microprocessors have evolved from 4-bit processors in the first microprocessor-base engine controller to 16-bit processors in most production engine controllers today and 32-bit processors in some advanced controllers. Control system functions are no longer limited to basic air/fuel ratio control and extend to include idle control, powertrain control and self-diagnostics.

This thesis details the first step in the development of a prototype engine controller from theory to implementation. The project was done in conjunction with the 1997

Chrysler Propane Vehicle Competition. The particular vehicle used as design target platform is a 1995 Chrysler Minivan, which was converted to operate on propane. A highly hardware-configurable controller was built. Software was developed to control engine air/fuel ratio and fuel system operation.

In Chapter 2, a brief introduction is given on the operation and control of spark-ignition engines. Chapter 3 describes the configuration of the Minivan engine system, its sensors and actuators. Chapter 4 details the hardware aspect of the engine controller. Chapter 5 discusses the development of the engine control algorithm and its software implementation. Finally, conclusions and recommendations for future work come in Chapter 6.

CHAPTER 2

ENGINE CONTROL BASICS

Over the last decade the ever tighter requirements of low emission and high performance have forced a trend towards more and better engine control and subsystem management. Modern engine control systems have become ever increasingly sophisticated. Before further discussing the development of the engine controller (named TTUCM in this project), the basic operation of a spark-ignition engine and some control problems associated with it will be presented.

2.1 Operation of SI Engine

Among other engine types, only the four-stroke spark ignition (SI) engine is discussed here. In a four-stroke SI engine, the fuel is ignited by spark; one engine cycle involves four strokes of a piston. Its operating cycle can be explained by reference to Figure 2.1 [3].

1. The induction stroke. The inlet valve is open, and the piston travels down the cylinder, drawing in a charge of air-fuel mixture.
2. The compression stroke. Both valves are closed, and the piston travels up the cylinder. As the piston approaches top dead center (TDC), spark ignition occurs.
3. The expansion or power stroke. Combustion propagates throughout the charge, raising the pressure and temperature, forcing the piston down. At the end of power stroke the exhaust valve opens.

4. The exhaust stroke. The exhaust valve remains open, and as the piston travels up the cylinder the remaining gases are expelled. At the end of the exhaust stroke, the exhaust valve closes.

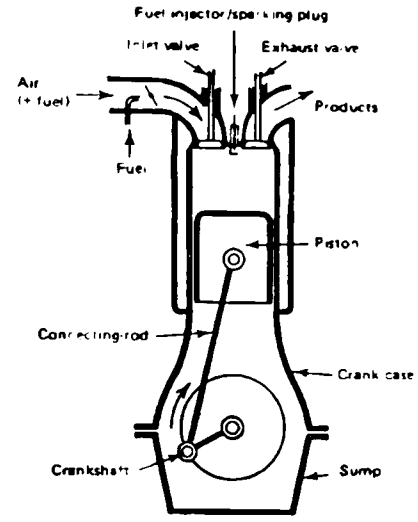

Figure 2.1 A Four-stroke SI Engine [3].

2.2 Basic Engine Control

The basic objectives of the engine control systems are to minimize exhaust emissions and fuel consumption while maintaining good driverability for all operating conditions. To achieve these goals requires coordinated control of several engine subsystems.

2.2.1 Fuel Control

Fuel control, which includes fuel delivery control and fuel metering, is the most important task of an engine control system. It has decisive influences on many aspects of engine performance, e.g., emission, fuel economy and driverability

2.2.1.1 Stoichiometric Ratio

During the power stroke, the air-fuel mixture is ignited by a spark. Chemical energy in the fuel is converted into kinetic energy of the piston through the combustion process. The greatest effect on the combustion process comes from the mass ratio of air to fuel. The air/fuel ratio is often described in terms of the excess-air factor known as lambda (λ) [4]:

$$\lambda = \frac{\text{actual air / fuel ratio}}{\text{stoichiometric ratio}} \quad . \tag{2.1}$$

The stoichiometric ratio is the chemically correct air/fuel ratio for complete combustion. It is fuel-dependent, 14.7 for gasoline and 15.8 for propane.

The air/fuel ratio affects the engine's fuel consumption and power output, as indicated in Figure 2.2, where sfc stands for specific fuel consumption, and bmep is an acronym of brake mean effective pressure, a measure of engine work output. The mixture strength for maximum power is about 10 percent on the rich side of the stoichiometric ratio, while best fuel economy is obtained with a mixture strength about 10 percent lean of the stoichiometric ratio [3].

Exhaust emission is very sensitive to the air/fuel ratio. The composition of exhaust gas varies as a function of λ. Modern emission control systems include a three-way-catalyst converter which can transform all three regulated exhaust gases: HC, CO and NOx into less harmful CO_2 and H_2O. The efficiency of the catalyst is very sensitive to air/fuel ratio. Even a 1% deviation in air/fuel ratio results in a 50% degradation of

converting one or more pollutants [5]. Resulting tailpipe exhaust emissions reach a minimum at stoichiometric ratio (λ=1), as can be observed in Figure 2.3.

Considering all the factors discussed above, the stoichiometry of air/fuel ratio yields a good tradeoff among engine's performance, fuel economy and emission. Although most of the data shown above was obtained from gasoline engines, the conclusion is the same for alternative fuel engines. For some alternative fuels such as propane, a special catalytic converter must be used for best results.

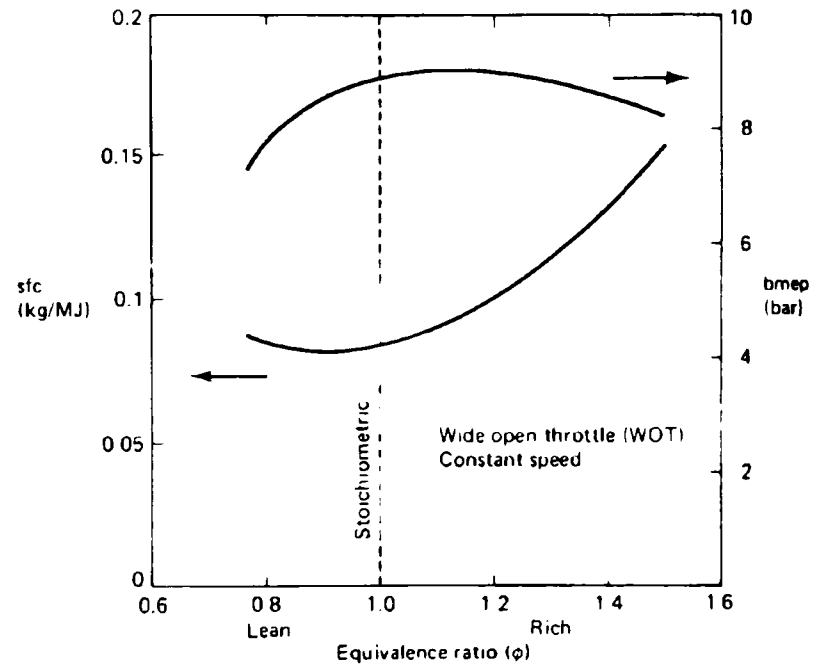

Figure 2.2 Response of Specific Fuel Consumption and Power Output to Changes in Air/fuel Ratio [3].

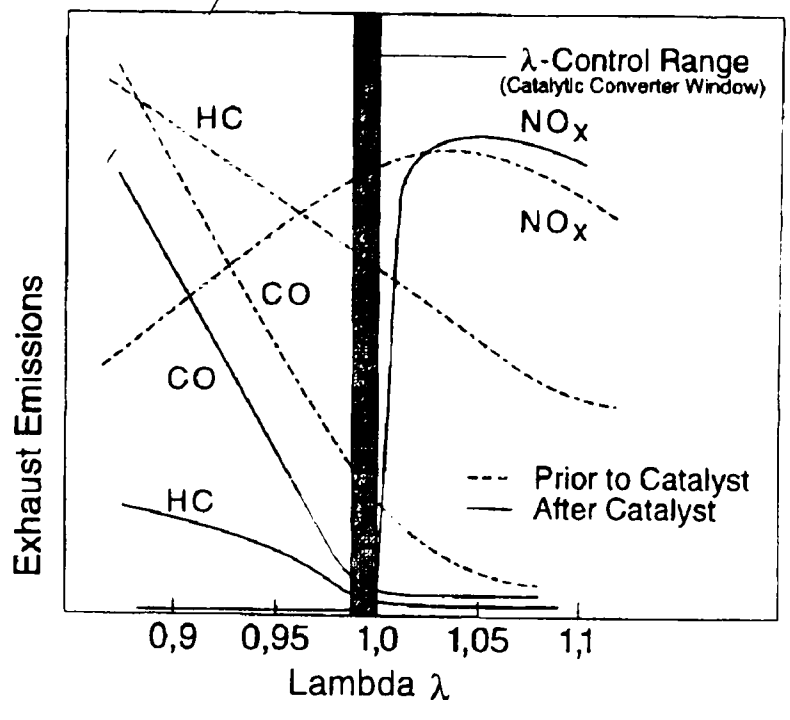

Figure 2.3 Lambda Effects on Exhaust Emissions Prior to and After Catalyst Treatment [4].

2.2.1.2 Air/fuel Ratio Control

In the last section, the stoichiometric ratio is shown to be the optimal air/fuel ratio. This section will discuss how to control the air/fuel ratio around stoichiometry.

In order to deliver appropriate amounts of fuel and obtain the stoichiometric air/fuel ratio, the engine control system must determine the amount of incoming air, known, as air charge.

$$Fm = \frac{Am}{\text{target air / fuel ratio}} \tag{2.2}$$

where Am is the air mass inducted in one engine cycle and Fm is the fuel mass to be delivered in one engine cycle.

There are three methods commonly used for determining the air charge: speed-density, air flow and air mass [4]. The speed-density method is used in the Minivan engine. The configuration for speed-density method is shown in Figure 2.4.

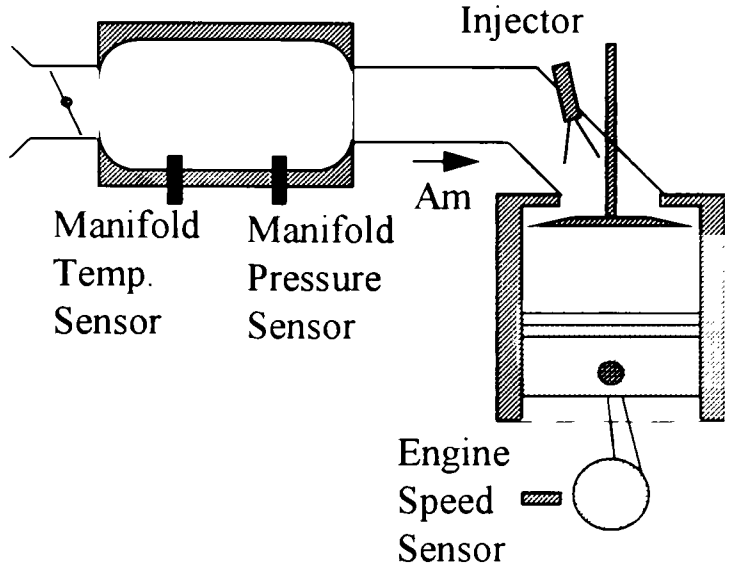

Figure 2.4 Speed-density Configuration

With the speed density method, air charge Am is determined by [5],

$$\mathrm{Am} = \frac{\mathrm{V}_e \cdot \eta_{vol} \cdot P_{\mathrm{m}}}{\mathrm{R} \cdot \mathrm{T}_{\mathrm{m}}} \tag{2.3}$$

where Ve is the engine displacement, Pm is the intake manifold pressure, Tm is the intake air temperature, and R is the universal gas constant. The volumetric efficiency η_{vol} is a function of many variables, but is most dependent on manifold pressure and engine speed for a given intake geometry. Thus Am is seen to be a function of manifold pressure and engine speed [5].

$$\mathrm{Am} = f(\mathrm{Pm}, \omega_e) \tag{2.4}$$

The function is instantaneous. Given instantaneous measurement of Pm and ω_e, the instantaneous air charge can be determined. Due to its non-linearity, the function is usually captured in a two-dimensional lookup table.

However, in the presence of model error, engine aging and disturbances such as Exhaust Gas Recirculation (EGR), the air charge is known accurately only to a certain degree. The lookup table has to be supplemented by feedback control to eliminate steady-state error. A simple air/fuel control system is shown in block diagram form in Figure 2.5

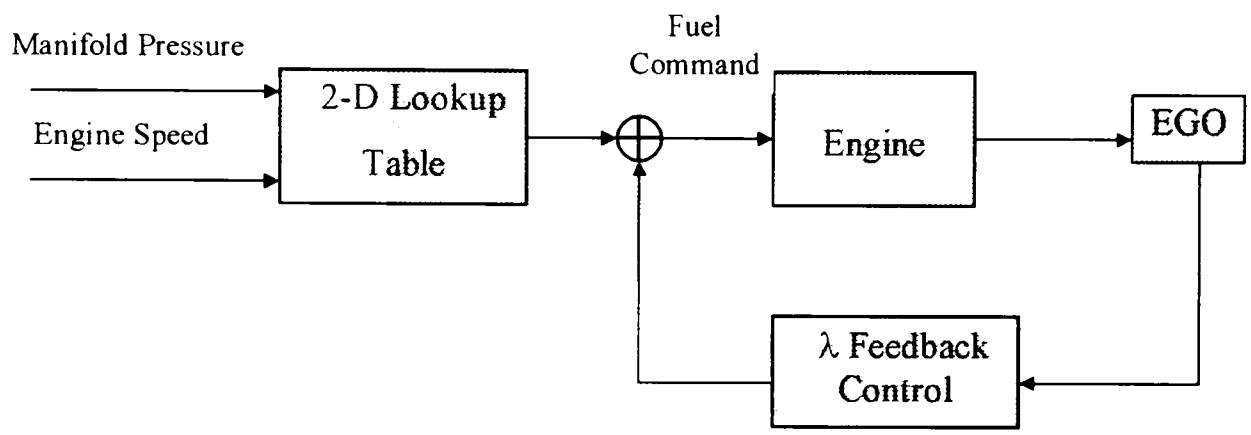

Figure 2.5 Block Diagram of Simple Air/fuel Control System

An exhaust gas oxygen sensor (EGO) is installed in the engine exhaust system upstream of catalytic converter. The EGO responds to the oxygen content of the exhaust and provides feedback information on the actual air/fuel ratio.

Under steady state conditions, the control system fine-tunes its fuel command using feedback from the EGO to obtain the setpoint air/fuel ratio. Under transient conditions, the exhaust gas transport delay and EGO lag will result in poor driverabilty and large air/fuel ratio excursions if only EGO feedback control is used. An anticipatory control strategy, which uses manifold pressure and engine speed to determine approximate

fuel requirements from the above mentioned lookup table, allows for rapid response to changes in operating conditions.

In a real engine system, air/fuel ratio control is complicated by many other factors, which include sensor and signal filtering lag, transport delay and fuel dynamics. The impact of these factors on system performance and solutions to these variations are introduced as needed in later chapters.

2.2.1.3 Engine Control Modes

With a stoichiometric air/fuel ratio, an engine operates optimally in terms of power output, fuel economy and emission. However, under some conditions, other factors are more important.

2.2.1.3.1 Engine Crank and Start. For engine start, the goal is to get the engine started with minimal delay. The air/fuel mixture is enriched to compensate for the unstable combustion of fuel during crank and start. For liquid fuel, further enrichment is necessary due to poor fuel vaporization and a "wall wetting" effect which decrease the amount of usable fuel.

2.2.1.3.2 Engine Warm-Up. For engine warm-up, the goal is to keep the engine operating smoothly while warming-up the engine and exhaust to operating temperature quickly. Before the lambda sensor is warmed up and ready, the engine runs rich in open-loop to guarantee a smooth operation margin. For liquid fuel, further enrichment is required depending on engine temperature.

2.2.1.3.3 Wide Open Throttle (WOT). Maximum torque and power output is expected at WOT. Target λ is set at 0.9 to 0.95 to deliver maximum torque output. Emission and fuel economy are temporarily sacrificed.

2.2.2 Ignition Control

The ignition timing is defined as the crankshaft angle before top dead center (BTDC) at which the ignition spark occurs [4]. The timing has an effect on the engine's power output, efficiency and emissions. A typical response for power output (and also efficiency) is shown in Figure 2.6, where bmep stands for mean brake effective pressure, and η_b, brake thermal efficiency. With the ignition timing at minimum advance for best torque (MBT), the engine operates with maximum torque output and knock margin. Knock is a kind of violent resonance in engine block, which may cause engine damage.

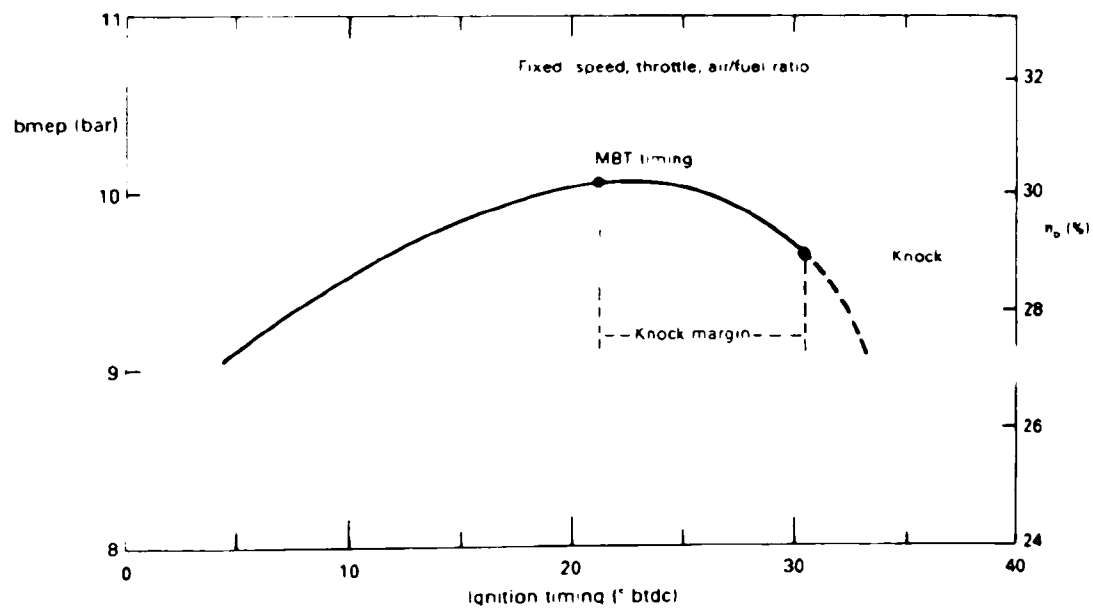

Figure 2.6 Effects of Ignition Timing on the Output and Efficiency of a SI Engine [3].

Optimal ignition timing, which is very close to MBT, varies with manifold pressure and engine speed [3]. It also depends on fuel characteristics. The more slowly the fuel burns, the more spark advance. Basic ignition timing control uses lookup tables calibrated through extensive engine test at all combinations of load and speed.

CHAPTER 3

MINIVAN ENGINE SYSTEM

3.1 Introduction

The platform on which the TTUCM was designed is a 1995 Chrysler Town & Country Minivan which has been converted to run on propane. The Minivan is equipped with a 3.3 liter, 6-cylinder sequentially fuel-injected engine, in a speed-density configuration. Figure 3.1 shows a block diagram of the Minivan engine system, with the sensors and actuators that are relevant to the engine control. All of the original sensors and actuators, except for the fuel injectors were used in the TTUCM system.

The original control system consists of three major modules: the Powertrain Control Module (PCM), the Transmission Control Module (TCM) and the Body Control Module (BCM). The TTUCM was designed to take over some of the fuel-related PCM functions.

The PCM controls the engine system operation. It regulates the ignition timing, fuel injection, air/fuel ratio, emission control devices, cooling fan, charging system, idle speed and vehicle speed control [6]. The PCM communicates with the other control modules and sub-modules via a serial port called the CCD bus The PCM also implements the On-Board Diagnostics II (OBDII).

This chapter describes some of the sensors and actuators in the Minivan engine control system as well as their interaction with the PCM. This knowledge provided the basis on which the TTUCM was designed.

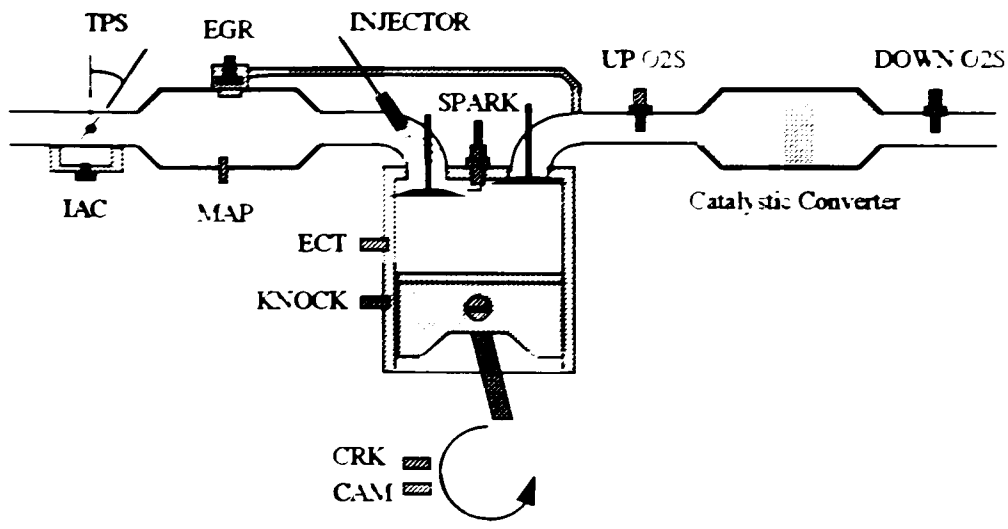

Figure 3.1 Minivan Engine System

3.2 Sensors

3.2.1 Crankshaft and Camshaft Position Sensors

Camshaft and crankshaft position sensors provide engine cycle synchronization and cylinder identification. The engine controller uses these signals to find the position of each cylinder, and then determines the injection/ignition sequence.

The crankshaft converts the reciprocating motion of the piston into rotary motion. The crankshaft rotates two revolutions for every engine cycle. The camshaft is geared to the crankshaft and rotates one revolution for every engine cycle. The camshaft controls the opening and closing of the valves

The position sensors for the crankshaft and camshaft are integrated digital Hall-effect devices. When aligned with metal, they output a low voltage, otherwise they are set to a high voltage. Powered by +8V DC, they can provide very clean TTL compatible signals(0.5-5V). There are notches on both crankshaft and camshaft sprockets. As the shafts rotate and these notches pass underneath the sensors, pulses are generated.

A sample of synchronized crankshaft and camshaft position pulses is shown in Figure 3.2. Each group of camshaft pulses is followed by four crankshaft pulses. The unique camshaft pulse pattern identifies which cylinder the following four crankshaft timing pulses correspond to, while the crankshaft pulses mark the accurate positions of that cylinder, namely, 69°, 49°, 29°, 9° BTDC [6]. By keeping track of these pulses, the engine controller can synchronize its control to engine events.

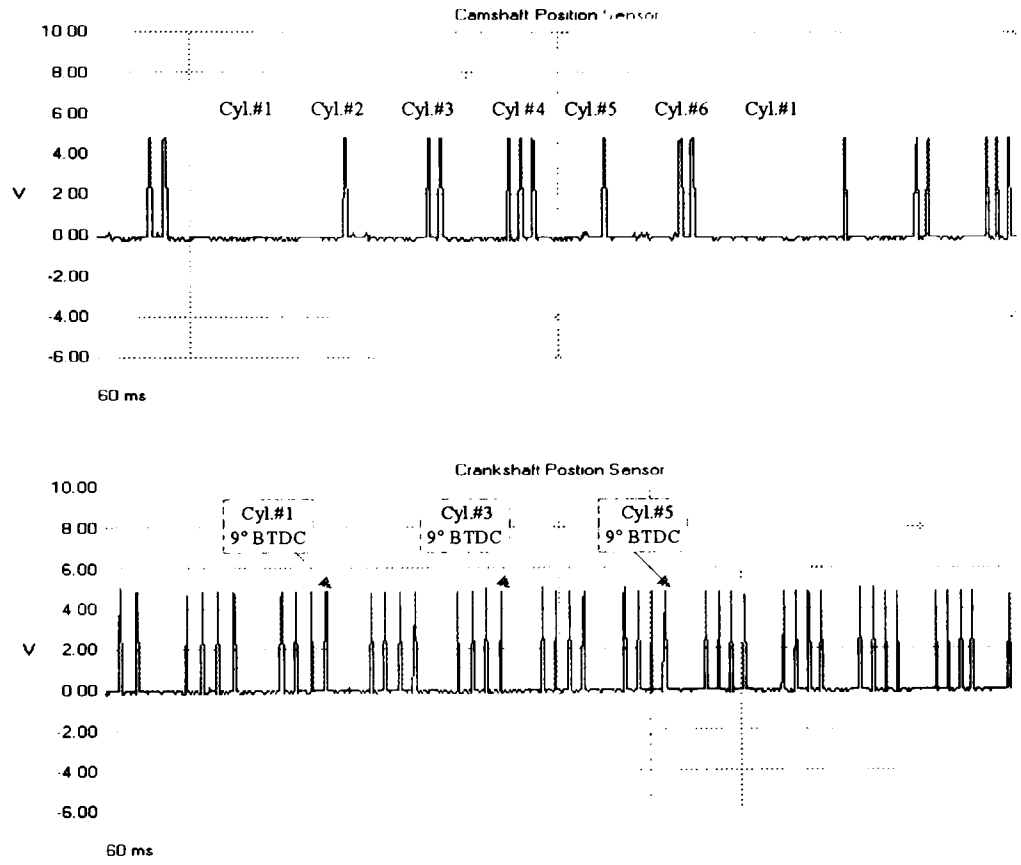

Figure 3.2 Camshaft and Crankshaft Position Pulses

3.2.2 Manifold Absolute Pressure (MAP) Sensor

The MAP sensor is crucial in the speed-density system. It provides information on engine load, which is one of the most important engine parameters. The MAP sensor used in the Minivan engine is believed to be an integrated piezoelectric pressure sensor. It receives +5V DC from the PCM and outputs a low-impedance voltage that is linearly

related to the intake manifold absolute pressure [6]. A static characteristic curve for the MAP sensor is as shown in Figure 3.3. This type of pressure sensor is fairly fast in response, with a typical 20ms response time. The test data shown in Figure 3.4 gives a close estimate of τ=25 ms. The sensor is fast enough for engine applications, and the lag of sensor itself is negligible.

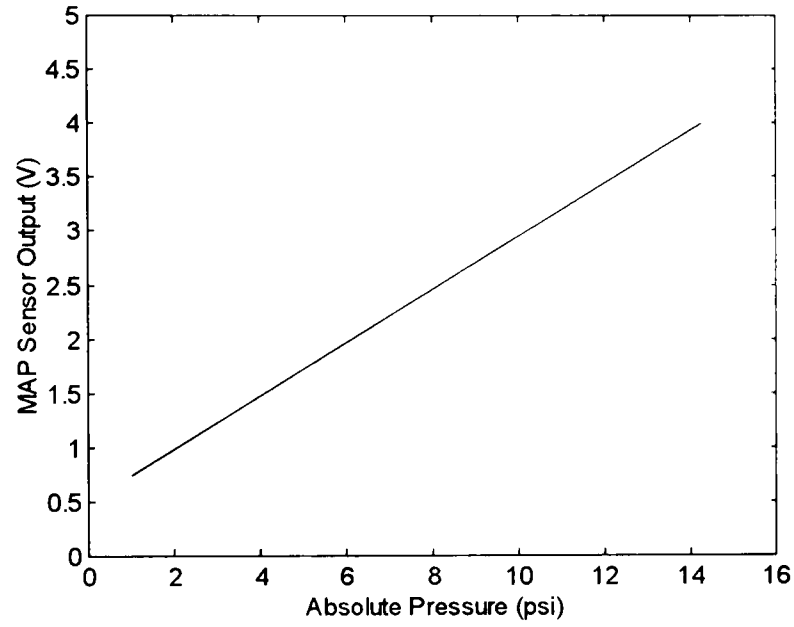

Figure 3.3 Static Characteristics of MAP Sensor

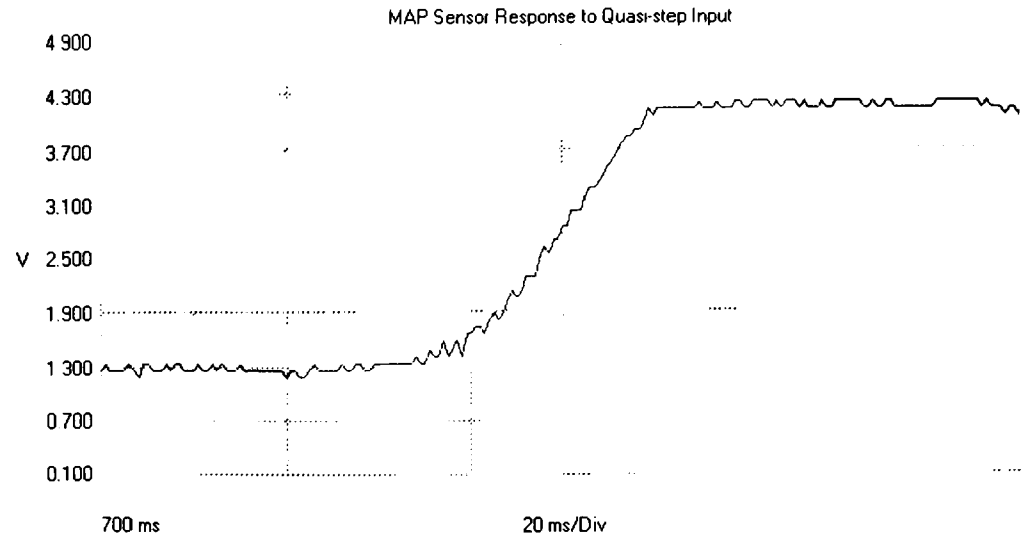

Figure 3.4 MAP Sensor Response to Quasi-step Input

3.2.3 Engine Coolant Temperature (ECT) Sensor

Engine temperature affects the engine operation, and is another important engine control parameter. The ECT sensor provides information on engine temperature. The engine controller uses this information to calculate temperature correction coefficients, such as, cold enrichment.

The ECT sensor used on the Minivan engine is believed to be a negative temperature coefficient (NTC) thermistor. The PCM supplies +5V DC to it through a series resistor. A voltage which varies as the ECT resistance changes is, thus, present across the ECT sensor. The PCM uses this voltage to determine engine temperature.

Interestingly, the PCM switches the series resistor as the ECT changes to obtain both a wide sensing range and high resolution. When the engine is hot and the ECT resistance is small, the PCM will switch to a lower resistor to compensate for the resolution loss at the high temperature end; otherwise a higher resistor is used. This process produces a hysteresis, as shown in Figure 3.5, in which one ECT voltage corresponds to two distinct temperatures. This unique situation makes it difficult for a parallel controller to share ECT sensor information with the PCM.

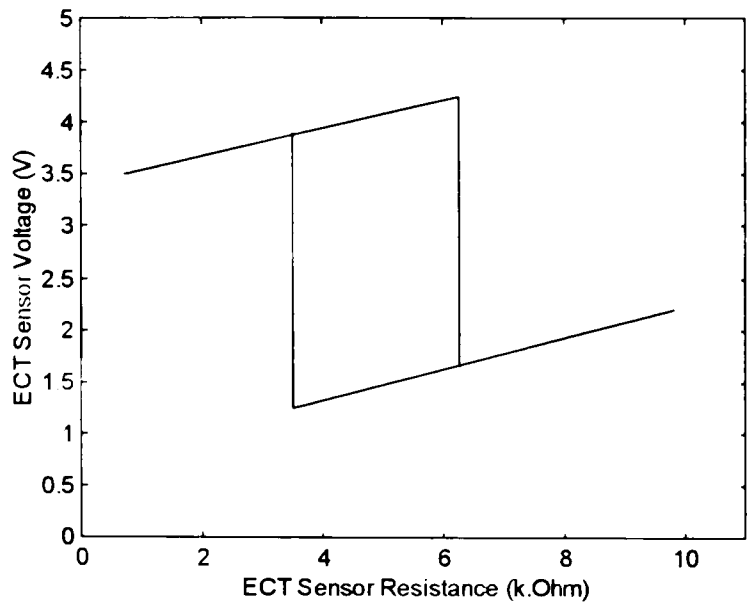

Hot Mid Cold

Figure 3.5 ECT Sensor Voltage

3.2.4 Heated Oxygen (O_2S) Sensor

The O_2S sensor provides feedback on air/fuel ratio. The O_2S sensor used in the Minivan engine is believed to be a switch type lambda sensor. Its typical output characteristic is shown in Figure 3.6. The sensor is primarily binary in nature, especially in the interesting region around $\lambda=1$. Only whether the air/fuel ratio is rich or lean is indicated. It is very hard to determine the actual air/fuel ratio. The nominal cross voltage ($\lambda=1$) is 0.45V (for gasoline).

The sensor has a fairly fast response time, in the neighborhood of 50ms. The sensor lag is thus of secondary significance compared to the longer exhaust gas transport delay [4]. However, asymmetry in the response times on both sides of the stoichiometric ratio, combined with possible cross voltage fuel-dependency, necessitates the biasing of the sensor output to eliminate a lambda shift. The emission data in Figure 3.7 indicates the effect of biasing.

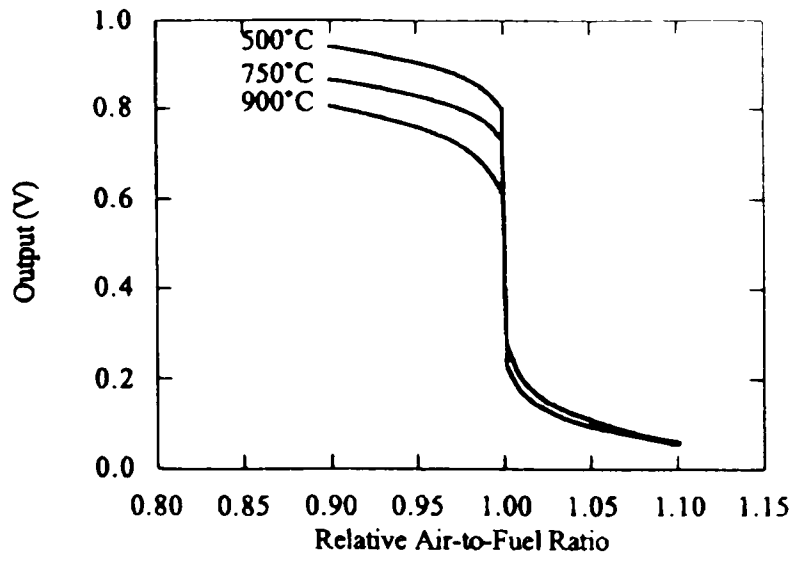

Figure 3.6 Typical Output Characteristics of a Lambda Sensor [5]

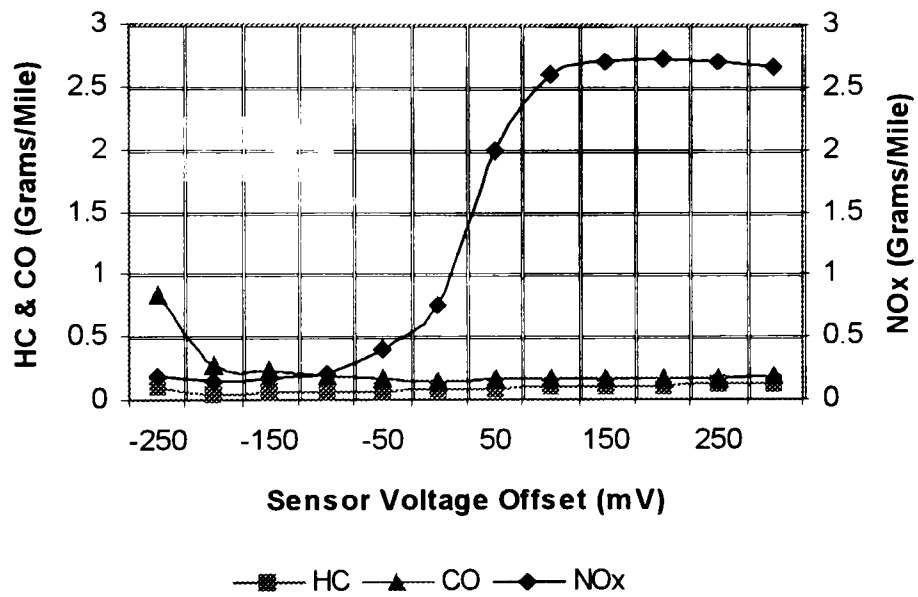

Figure 3.7 Effects of O_2S Sensor Biasing on Emissions

The O_2S sensor is essentially a high impedance voltage generator. The fully operational sensor was observed to have an impedance of over 100kΩ. A high input-impedance buffer is thus needed to interface the sensor. Experiment results indicate that the PCM interfaces the O_2S sensor in a configuration as shown in Figure 3.8.

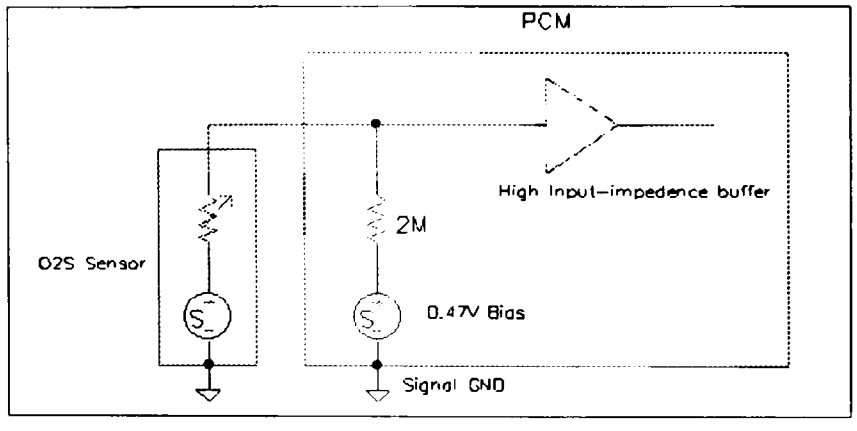

Figure 3.8 PCM O_2S Sensor Interface

Before being fully warmed-up, the sensor is not conductive (very high internal impedance), and its output is overridden by the PCM internal bias. A 0.47V bias voltage appears on the sensor wire. As the sensor reaches its operating temperature and becomes conductive, its output is able to override the PCM internal bias and appears on the sensor wire. Due to its switching characteristic, the output of an operational sensor spends very little time at 0.47V. It is either 0.2V or 0.8V most of time. The PCM can thus determine the sensor's readiness simply by sampling its output. If the output voltage stays very close to 0.47V, the sensor is not ready.

3.2.5 Throttle Position Sensor (TPS)

The TPS is a variable resistor that provides the PCM with a voltage representing throttle blade position. Its output varies from 0.5V at idle to 3.9V at Wide Open Throttle (WOT). Engine controller interprets the TPS output to derive the driver's intention.

3.3 Actuators

All the actuators are connected to the battery positive after the engine starts up. PCM controls the actuators by providing a ground path as shown in Figure 3.9. The final

stage of control circuit might be either a power transistor or a relay depending on the switching frequency involved.

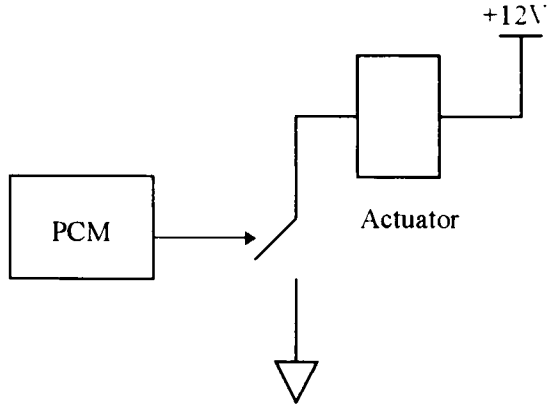

Figure 3.9 PCM Control of Actuators

3.3.1 Fuel Injectors

There are six injectors, one for each cylinder. Each injector is controlled separately. Injection timing and pulse width can be optimized for each individual cylinder. The original fuel injectors were 12 ohm electrical solenoids [6]. The BKM gaseous injectors used in the converted Minivan have a much lower resistance of 1 ohm. The engine controller controls the fuel injection order, timing and pulse-width by switching individual solenoids on and off. On-board diagnostic detects failed or defective of fuel injectors. The original injectors must be connected to PCM to avoid the indication of an error by the PCM, even when the fuel injection is actually controlled by TTUCM.

3.3.2 Ignition Coil

The Minivan uses a 'wasted spark' distributorless ignition system. There are three coils that each fires two spark plugs every power stroke. One spark occurs in the cylinder under compression, while the other fires in the cylinder in the exhaust stroke [6]. The

PCM controls the charge and firing of each coil. The charging time is a constant 5ms, independent of engine state.

3.3.3 Exhaust Gas Recirculation (EGR) Valve

The EGR dilutes the intake air/fuel mixture with inert exhaust gas to reduce combustion strength. It helps to improve fuel economy and reduce NOx emission. The Minivan engine uses a kind of electronic transducer valve. When the valve solenoid is de-energized, the EGR is on and its strength is mechanically regulated by a back-pressure transducer. More accurate control can be obtained with the use of electrically regulated valve.

3.4 Switches

Switch signals indicate the postions of some switches or relays which have an effect on control decisions. They are all 0-12V on/off signals.

3.4.1 Automatic Shutdown Relay Output

The Automatic Shutdown (ASD) relay supplies +12V power to critical components, such as, the ignition coils, the fuel injectors, etc. The PCM will de-energize the ASD relay if it does not receive camshaft or crankshaft signals for one second or detects fatal system failures. In this light, the ASD relay output serves as an indication of engine system functionality. It is +12V when the relay is energized, and 0V otherwise.

CHAPTER 4

TTUCM CONTROLLER HARDWARE

4.1 Introduction

The TTUCM controller is expected to eventually be able to take over all of the PCM control functions and completely replace the PCM. However, at this preliminary development stage, the TTUCM operates in parallel with the stock PCM in a cooperative fashion. The TTUCM takes over the PCM functions which are fuel related and optimizes them for the specific fuel being used, while leaving the other control functions to be done by the PCM. On one hand, the TTUCM is able to access the stock sensors and control the actuators involved; on the other hand, the TTUCM does not present interference to the normal operations of the PCM and original sensor system. To preserve system integrity, efforts were taken to prevent the PCM's detection of errors caused by removing the PCM's control over some subsystems and replacing it with TTUCM's control.

The block diagram of engine-PCM-TTUCM system is shown in Figure 4.1. All the engine sensor and switch signals are basically voltage signals. They are shared between the PCM and TTUCM by wire tapping. The PCM-to-actuator connections were broken and grouped. Each group of wires was put into a pair of connectors--one on the PCM end and the other on actuator end. Another connector, identical to the PCM end connector, groups the corresponding TTUCM control signals together. With this setup, the control of any specific actuator group, such as the injector group and the ignition group, can be conveniently switched back and forth between the PCM and TTUCM.

When the TTUCM controls an actuator group, the PCM control signals for that actuator group should be connected to a dummy load which is basically the same type of actuator but not connected to the engine system. The purpose of this practice is to prevent the PCM from sensing the loss of control and giving a malfunction indication.

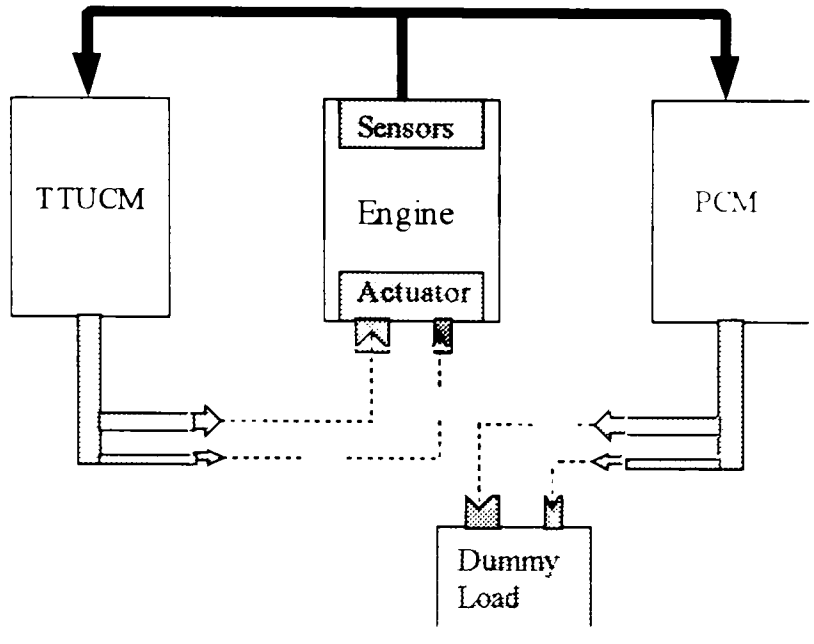

Figure 4.1 Engine-PCM-TTUCM System

Figure 4.2 is a block diagram of the TTUCM controller. The TTUCM controller consists of three submodules: the microprocessor submodule, the interface submodule and the relay submodule. The core of the TTUCM is a Motorola MC68F333 microcontroller. A 32-bit microprocessor combined with powerful peripheral subsystems, the MC68F333 targets high-end automotive engine control applications. The MC68F333 system is implemented in a modular evaluation board (MEVB). The MEVB provides the essential timing, I/O and other support circuitry for the microprocessor, and serves as a basic system for fast prototyping and evaluation. The interface submodule provides reliable power for the MEVB, conditions all the engine signals before input to the MEVB and provides high-current drivers for some engine system actuators as well as relays in the

relay submodule. The relay submodule provides relay-control for some engine system actuators.

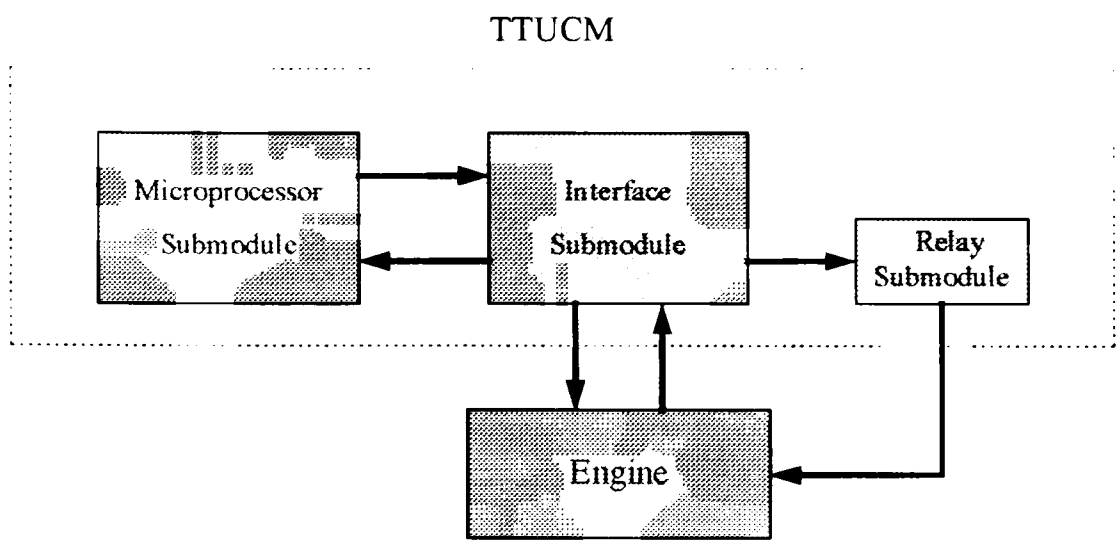

Figure 4.2 TTUCM Block Diagram

Due to the development nature of this project, the TTUCM controller was designed to provide maximum degrees of flexibility, expandability and portability. New sensors and actuators can be easily incorporated into the system as the development goes on and new control functions are added. This is achieved by the selection of a powerful microcontroller and a special design of the I/O interface circuits, as is described in the later sections.

The TTUCM can handle up to 18 input signals of a variety of formats and 16 high-current output signals. Although only part of this capabilities are currently used in the control software, most of the I/O channels have been assigned and connected to the engine signals which are expected to be used in future development. These signals are listed in the Appendix along with the interface circuits used with them. Some spare channels are also available for new sensors and actuators that are not used in the current engine system.

This chapter deals specifically with the TTUCM controller hardware. Three TTUCM submodules will be introduced in more detail in the following sections.

4.2 Microprocessor Submodule

The microprocessor provides sophistication and reliability. It detects and processes sensor input signals, and responds by asserting control signals to the actuators. Many control tasks are considered impossible without microprocessors, and microprocessor has become an indispensable component of many control systems in use today.

The TTUCM is a microprocessor-based embedded controller. The core of the system is a Motorola MC68F333 microcontroller. It is implemented on a product evaluation board M68MPBF333C.

4.2.1 MC68F333 Architecture

The MC68F333, a 32-bit highly-integrated microcontroller, combines high-performance data manipulation capabilities with powerful peripheral subsystems. Using a fully static design, it operates with a system clock frequency from 0 Hz up to 16.78 MHz [7]. Figure 4.3 is a functional diagram of the MC68F333

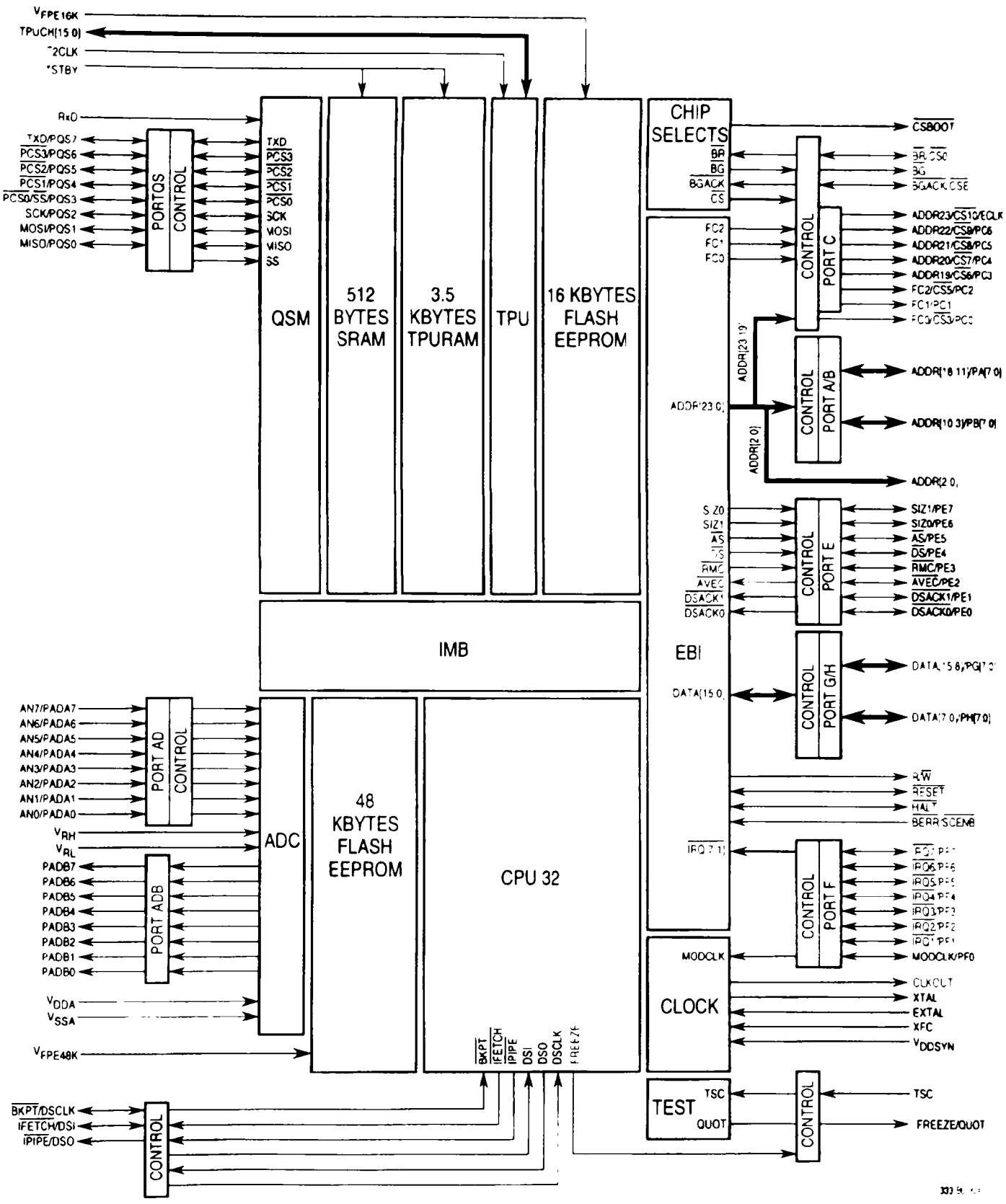

Figure 4.3 MC68F333 Block Diagram [7].

The MC68F333 adopts a modular design. It incorporates a 32-bit CPU (CPU32), a single-chip integration module (SCIM), an 8-channel, 10-bit analog-to-digital converter (ADC), a time processor unit (TPU), a queued serial module (QSM), a 512-byte standby RAM (SRAM), a 3.5-Kbyte RAM with TPU emulation capabilities (TPURAM), and two flash EEPROM modules (FLASH16, FLASH48). These modules are connected to the CPU32 by the intermodule bus (IMB) [7].

The CPU32, the 32-bit instruction processing module of the M68300 family, is based on the industry-standard MC68000 processor. It is fully upward object code compatible with M68000 family, which allows the use of the extensive software base for the Motorola M68000 family. It has many features of the MC68010 and MC68020, as well as unique features suited for high-performance controller applications. With the flexible addressing modes and enhanced instruction set, the CPU32 will efficiently support high-level language (HLL), which is preferred as control programs become larger and more complex [7, 8].

The peripheral subsystem of the MC68F333 is control-oriented. It has many unique features designed for high-performance control applications.

The single-chip integration module (SCIM) consists of system configuration and protection, system clock, external bus interface and chip-select block. Typical micro-processors require additional hardware to provide external chip-select signals. The MC68F333 includes nine programmable chip-select circuits that can provide access to external memory and peripherals. Thus, system integration is greatly simplified. For critical applications like automotive engine control, system reliability is an important

consideration. The SCIM provides improved system safe-failure and graceful recovery capabilities by featuring a bus monitor, a halt monitor, a spurious interrupt monitor and a software watchdog

The analog-to-digital converter (ADC) module is a unipolar, successive-approximation converter with eight modes of operation, a maximum of eight analog channels and selectable 8- or 10-bit resolution [9]. Conversion can be executed once or continuously. Monotonicity is guaranteed for both 8- and 10-bit conversions. With a 16.78 MHz system clock, the ADC can perform an 8-bit single conversion in 8 microseconds or a 10-bit single conversion in 9 microseconds [9]. In the TTUCM, the ADC is used to convert the conditioned analog sensor signals, e.g., MAP, ECT and O_2S into digital data.

The time processor unit (TPU) performs simple as well as complex timing tasks, making it the latest advance in timer systems [10]. It greatly facilitates the crank angle-based engine control, which usually requires high CPU overhead.

The TPU is an intelligent, semi-autonomous microcontroller designed for timing control. It consists of two 16-bit free-running time bases, sixteen independent timer channels, a task scheduler, a microengine, and a host interface [7]. Operating independently and simultaneously with the CPU, the TPU services timing events and performs assigned timing functions which are otherwise done by CPU interrupt services. This feature significantly reduces the CPU overhead and increases system throughput. As a self-contained dedicated processor for timing control, the TPU provides high-resolution timing and reduced latency. All timer channels are identical and can be configured to

perform any time function, which makes the timer channel configuration very flexible. The TPU microcode ROM contains ten optimized and flexible factory-programmed time functions. These functions satisfy a wide variety of control applications while emulation capability is also supported for custom time function development. In the TTUCM, the TPU is used to synchronize the injection controls with engine events indicated by crankshaft and camshaft position signals, and measure engine speed. Factory-programmed time functions are used.

The MC68F333 offers a variety of high-speed on-chip memory modules. They can be used as regular memory in single-chip mode or for program code that must either execute at high-speed or is frequently executed, such as operating system kernels and standard routines [7]. They are disabled in TTUCM due to the availability of off-chip memory and the need to change the program code frequently.

4.2.2 Modular Evaluation Board M68MPFB333C

The MC68F333 is incorporated into the TTUCM through the Modular Evaluation Board M68MPFB333C. The M68MPFB333C is an economical system for debugging and evaluating the operation of MC68F333 microcontroller. By providing the essential microcontroller timing and I/O circuitry, the MEVB simplifies and speeds hardware and software evaluation [11]. Figure 4.4 is a hardware block diagram of the M68MPFB333C.

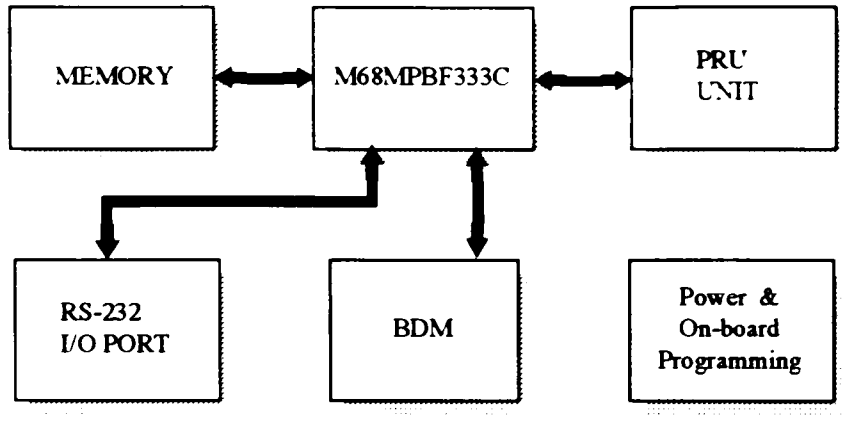

Figure 4.4 M68MPFB333C Hardware Block Diagram

The MEVB system consists of three components: Modular Platform Board (MPFB1632), Plug-in Microcontroller Personality Board (M68MPBF333C), and In-circuit Debugger (ICD32) assembly and development software. Only the Personality Board (MPB) is device- and package-specific while the Platform Board and ICD32 can be used with other M68300 family members. The MPB contains the microcontroller unit (MCU) and system clock. It plugs into the MAPI bus on the Platform Board.

The Modular Platform Board (MPFB) is equipped with on-board power conditioning and device programming voltage control, which allows the programming of external EPROM or MCU-internal EEPROM. The MPFB has three types of memory ports: Data RAM, Pseudo ROM and Fast RAM, and supports multiple memory device types (RAM, EPROM, Flash EEPROM), sizes (32KB-1MB), packages and port widths (byte/word) [11]. The TTUCM uses 64KB RAM in Data RAM port for data space; 64KB RAM in Pseudo ROM port for program space during the software development and EPROM after finalization. The memory configuration is done through jumper and chip-select programming. MPFB also includes a user-transparent Port Placement Unit (PRU) to rebuild I/O ports lost to address/data/control buses, and two RS-232C terminal I/O ports for user evaluation of the on-chip serial communication interface (SCI). On-board

logic analyzer pod connectors (for all MCU pins) and wire-wrap area facilitate the off-board connection to external circuits.

The Background Debug Mode (BDM) is a unique alternative CPU32 operating mode. During the BDM, normal instruction execution is suspended. The CPU-internal debugger, which is implemented in CPU microcode, receives external commands through the BDM port, performs a full sets of debug operations, and sends back the results through the BDM port. The in-circuit debugger ICD32 operates in full Background Debug Mode. Running on a host computer, it controls the CPU32 entering and exiting BDM, and communicates with the CPU-internal debugger via an ICD cable connecting the BDM port on MPFB and parallel port on host computer. Debugging is carried out by the CPU-internal debugger under the control of ICD32. No extra on-board debug firmware is needed, and the debugging does not consume MCU resources.

4.3 Interface Board

A custom-built interface board is used in the TTUCM. Intervening between the MEVB and the engine system, the interface board on one hand conditions and converts the engine sensor and switch signals into formats acceptable to the MEVB, and on the other hand, amplifies the MEVB control signals to drive the engine system actuators. It also provides reliable power for the MEVB.

The interface board accepts a variety of input signal formats: regular analog voltage, high-impedance analog voltage, high-speed direct digital input and isolation digital input. The high-current driver on the interface board is universal in that it can

control most of the regular automobile actuators. Each type of I/O interface will be discussed separately in the rest of this section.

To guarantee flexibility and room for future development, multiple generic signal paths are included for each type of interface. Special care was given to electrically isolate the small-current sensor paths from the noisy large-current control circuits, as well as to protect MEVB from being exposed to extreme voltages. Reliability and robustness were emphasized in the design.

4.3.1 Power, Ground and MEVB I/O Protection

A DATEL TWR-5/300-12/500-D48 DC/DC converter is used for powering the MEVB and the interface board. It receives 9-36V input and outputs 3 fully-isolated voltages: a +5V primary and ±12V auxiliaries. The I/O isolation is necessary since the signal ground of the interface board is isolated from the chassis ground. The primary +5V can source up to 3A current while the maximum MEVB-interface current rating is less than 2A. Numerous protection features are provided, including non-latching output current limiting, input overvoltage and reverse-polarity shutdown and output overvoltage clamping [12]. Compact design and good reliability make it ideal for this application.

To eliminate the potential interference and damage caused by large-current inductive actuators on the small-signal circuits, the signal ground of the interface board is fully isolated from the chassis ground. Sensor signals are referenced to the signal ground while switch signals and actuator control signals are referenced to the chassis ground as agrees with the PCM arrangement. However, the PCM signal ground and the chassis

ground are found to be internally connected together, which makes the isolation protection less effective.

To protect the MEVB from extreme voltages and shorts, a protection network is used for every off-board MEVB I/O as shown in Figure 4.5. This practice also minimizes Electrostatic Damage (ESD) and CMOS latch-up susceptibility. Resistor networks and Motorola MAD1103P monolithic diode arrays are used in the actual circuit.

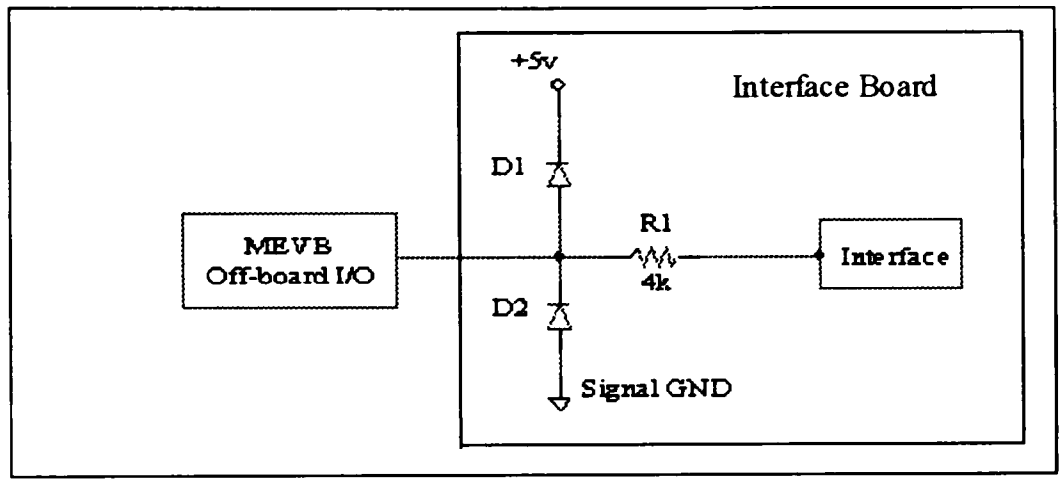

Figure 4.5 MEVB I/O Protection

4.3.2 Universal Isolation Driver

An universal isolation driver is used for driving engine actuators and relays. Figure 4.6 shows its schematic.

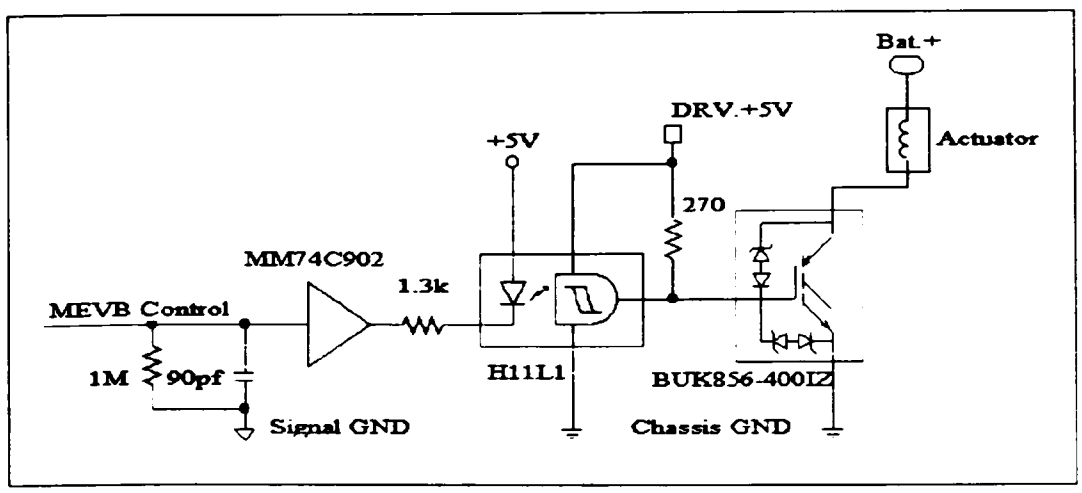

Figure 4.6 Universal Isolation Driver

The capacitor at the input, combined with the series resistor in the MEVB I/O protection network, serves as a low-pass filter to remove spikes on the line. Safe-failure is provided through the 1MΩ pull-down resistor. The MEVB control signal is fully isolated from the actuator circuit by a Motorola H11L1 optoisolator with Schmitt trigger output. As shown in Figure 4.6, there are two electrically isolated grounds. The H11L1 requires a low threshold current (1.6 mA max) and is output logic-compatible. Its output hysteresis provides better noise-immunity and more reliable operation. The MEVB I/O is HCMOS compatible. The MM74C902 non-inverting CMOS-TTL buffer provides an interface from the MEVB to the H11L1. An LM309 3-Terminal Voltage Regulator is used to provide +5V DC for the H11L1 circuit on the driver side, namely, DRV +5V. The BUK856-400IZ is a protected logic-level Insulated Gate Bipolar Transistor (IGBT) from Philips Semiconductors. Controlled by the logic-level (gate) signal, it can output up to 20A current (Collector current) and 100W power, which is sufficient for driving most of regular actuators used in an automobile. The device has built-in zener diodes providing active collector voltage clamping and ESD protection up to 2 kV [13], which eliminates the need for an external clamping diode when used with inductive loads and provides much more reliable operation.

There are, totally, sixteen universal isolation driver channels on the interface board, of which, ten channels are currently used to control the six fuel injectors, EGR valve and relays for Main Fuel Line Shutoff, Fuel Tank Top/Bottom Switch, and Staged Regulator Switch. Detailed information can be found in the Appendix.

4.3.3 Analog Interfaces

There are two types of analog interfaces on the interface board: general analog interface and high input-impedance analog interface. The interfaces buffer, scale and condition the voltage sensor signals from the engine system before being sent to the ADC in MC68F333. A schematic of the general analog interface is shown in Figure 4.7

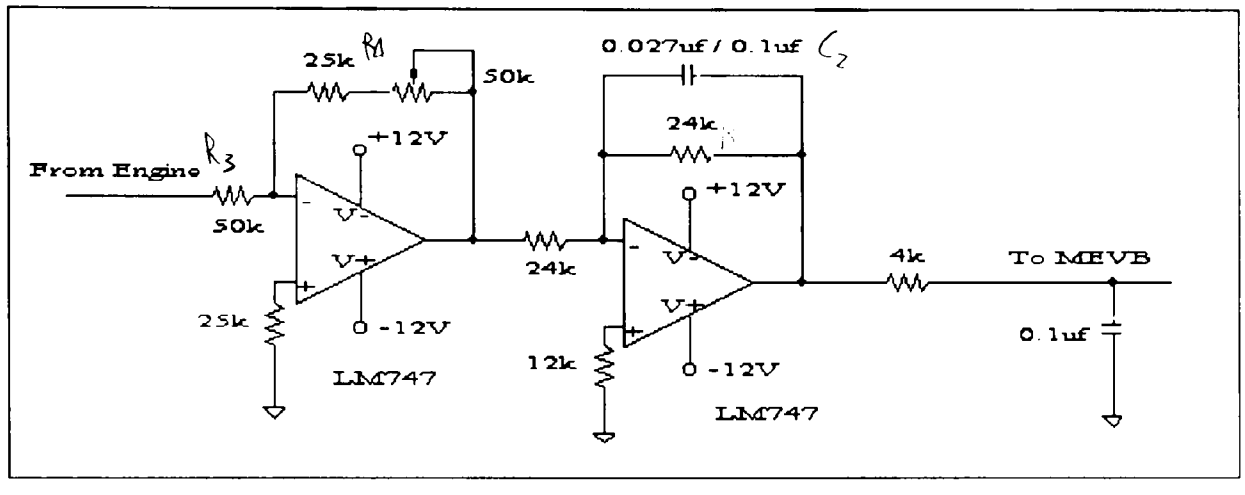

Figure 4.7 General Analog Interface

The circuit consists of two inverting amplifier stages. The first stage inverts and scales the input sensor signal, while the second stage inverts the signal again to restore the polarity. The scaling factor is $0.5 \sim 1.5$. The second stage also constitutes an active first-order low-pass filter. The cutoff frequency is 245Hz for fast signals, e.g., MAP, and 66Hz for slow signals, e.g., ECT. The 4kΩ series resistor at the output is from the MEVB I/O protection circuit, and the 0.1μf capacitor is actually installed close to the ADC pin on the MCU personality board. The time constant of the whole circuit is generally smaller than is required by the sensor speed and signal sampling. The filtering mainly targets the high frequency noise caused by the ignition.

Eight general analog interface channels are available on the interface board. Among them three channels have been assigned to the MAP, TPS, ECT. The scaling factors in these three channels are set at 1.

The high input-impedance analog interface is designed for the O_2S sensor. Its schematic is shown in Figure 4.8.

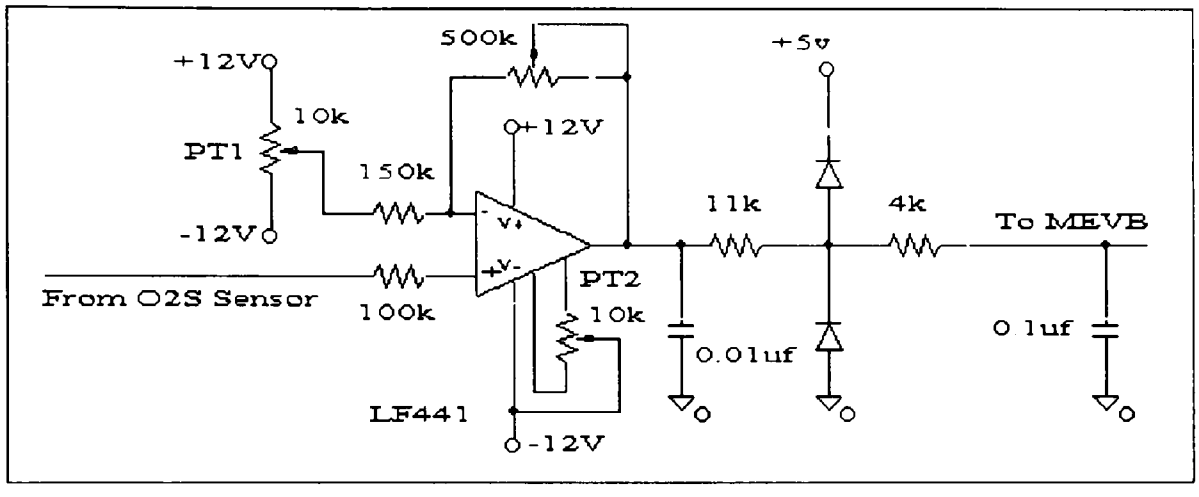

Figure 4.8 High Input-impedance Analog Interface

The circuit is basically a non-inverting amplifier with variable gain (1~4.3). A low power JFET input op-amp, LF441 has very high input resistance (10 GΩ), very low input bias and offset current (100 pA max). It also has a very low equivalent input noise voltage for a low power amplifier [14]. The O_2S sensor signal connects to the non-inverting input of the LF441, which makes the circuit's input impedance very high. Potentiometer PT2 balances the LF441. Potentiometer PT1 provides bipolar, hardware, O_2S sensor bias. The RC network at the output is similar to the one used in general analog interface.

There is one high input-impedance analog interface channel on the interface board. It is used for interfacing the upstream O_2S sensor. The scaling factor is set at 4 and hardware bias is not used (zero).

4.3.4 Direct and Isolation Digital Inputs

Direct digital inputs are used to buffer and trim logic sensor signals which are referenced to the signal ground, e.g., camshaft and crankshaft position sensor signals. Figure 4.9 shows its schematic.

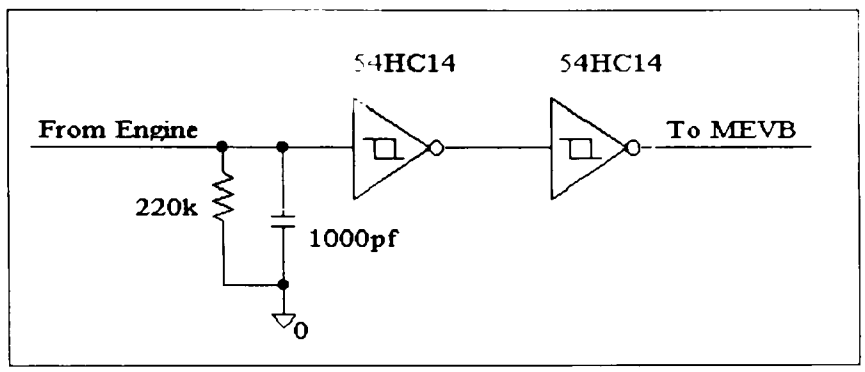

Figure 4.9 Direct Digital Input

Two inverters are used in series to preserve the signal polarity Since the camshaft and crankshaft position signals are both pulse signals, spurious glitches can confuse the controller and cause it to temporarily go out-of-lock and take conservative control actions. A Schmitt trigger was chosen for its improved noise immunity, and the RC network at the input also helps to filter out glitches.

Three direct digital input channels are available on the interface board, and two of them are currently used in the TTUCM for interfacing the camshaft and crankshaft position sensors.

The isolation digital input is used for switch signals which are referenced to the chassis ground. Figure 4.10 shows its schematic.

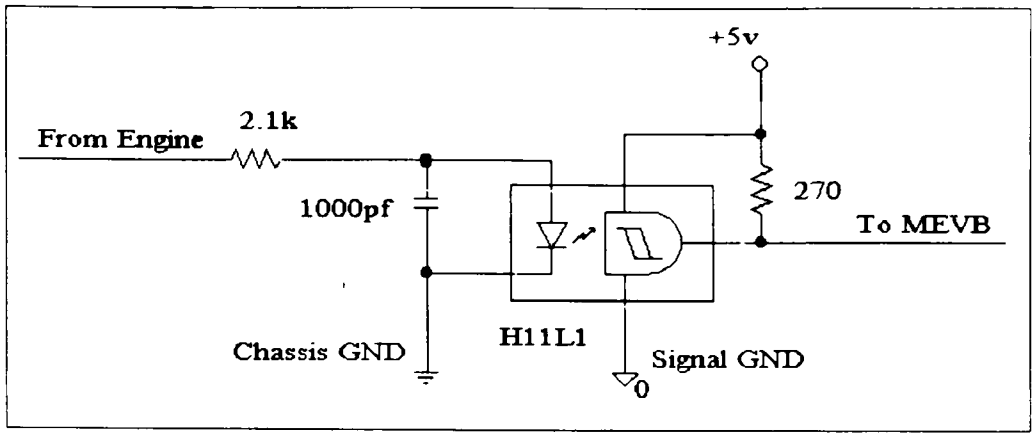

Figure 4.10 Isolation Digital Input

The H11L1 is again used to isolate the chassis ground and signal ground, and provide improved noise immunity. The RC network at the input helps to filter out glitches. When the switch input is low (0V) or floated, the circuit outputs a logic high (+5V); when the input is high (above 7V), it outputs a logic low (0.2V). The 7V input threshold is necessary for a reliability margin requirement, considering the battery voltage might drop to 8V during the prolonged cranking.

There are totally six isolation digital input channels available on the interface board. One channel is currently used in the TTUCM to interface the Automatic Shutdown Relay Output.

4.4 Relay Submodule

Relay submodule provides relay control for some actuators that are critical to the system operation and do not switch frequently. General-purpose automobile relays are chosen, and the universal isolation driver is used to control the relay coil. There are four relay circuits in the relay submodule and three of them are currently used for Main Fuel Line Shutoff, Fuel Tank Top/Bottom Switch and Staged Regulator Switch.

4.5 TTUCM Hardware Assembly

The printed circuit board (PCB) of the interface submodule was custom designed using PCAD 7.0 and built by a commercial manufacturer to insure good quality and reliability Included on the PCB are all the interface circuits described in previous sections as well as a small wire-wrap area for minor addition and modification. The IGBTs are actually attached to the case to insure good heat dissipation. They are electrically connected to the interface board through individual 2-pin connectors. The metal case provides the ground path.

The TTUCM is assembled into two steel sheet cases. One contains the MEVB and the interface board, and the relay submodule is enclosed in the other one to avoid its switching interference on the MEVB and interface circuits. The assembly uses connectors extensively to insure channel assignment flexibility as well as easy component detachment and replacement The MEVB and the interface board are connected by a 40-wire flat cable with socket connectors on both ends. The connections on the interface side are fixed, while the connections on the MEVB side were made using wire-wrap to allow flexible MCU I/O assignment.

The interface board connects to the engine system and relay submodule through a 36-pin D-sub connector. The majority of the interface channels and the D-sub pins have been assigned and connected to the engine signals that are expected to be used in the future development, although only part of them are currently used by TTUCM.

Detailed information on the TTUCM hardware can be found in the Appendix.

CHAPTER 5

TTUCM CONTROL SOFTWARE

5.1 Introduction

Today, microprocessors provide control systems with unprecedented flexibility and sophistication through software programmability. In a microprocessor-based control system, the control software implements the control algorithm and plays a decisive role in determining the system performance. The control software is the most dynamic component of the system. A minor change in the algorithm can sometimes significantly alter the behavior and performance of the whole system.

The software running on a microprocessor in a control system is often termed embedded. Several characteristics distinguish embedded control software from other general software. First, the embedded control software almost invariably operates in a real-time environment where real-time processing and fast response time are required. In this environment, special care has to be taken in the design of scheduling schemes and the coding of time-sensitive subroutines. Second, many control systems demand high system reliability. Embedded control software should be robust and provides for safe-failure, comprehensive error handling and recovery capabilities.

The main function of the TTUCM control software is engine air/fuel ratio control. Assembly language was chosen as the programming language for the current version of the control software. The software is still in its early stage of development, the amount of computation is minimal, and considerable low-level I/O operations as well as time-

sensitive operations are involved. Assembly language is known for its high execution speed and efficiency, and it is most convenient for direct low-level control. To facilitate future software development and maintenace, the modularity and hierarchy of the software were maximized. System reliabilty was given emphasis in the design. Automatic control data setup and adaptation were included to support easy software portability to other alternative fuel engines in the future.

This chapter covers the development of the TTUCM control software from theory to algorithm, from software implementations to experimental results.

5.2 Air/Fuel Ratio Control

5.2.1 Introduction

As suggested in Chapter 2, air/fuel ratio control is one of the most important tasks of the engine control system. The aim is to improve air/fuel ratio control accuracy over a period that may be as short as a fast engine transient or as long as the life of the engine. Besides the basic issues discussed in Chapter 2, several other problems associated with air/fuel ratio control in production engines have been identified in the literature [16, 22]. A good air/fuel ratio control system should address most of these issues depending on the actual engine configuration. Figure 5.1 shows a block diagram of a full-featured air/fuel ratio control system which takes into account all of the dynamics identified in the system.

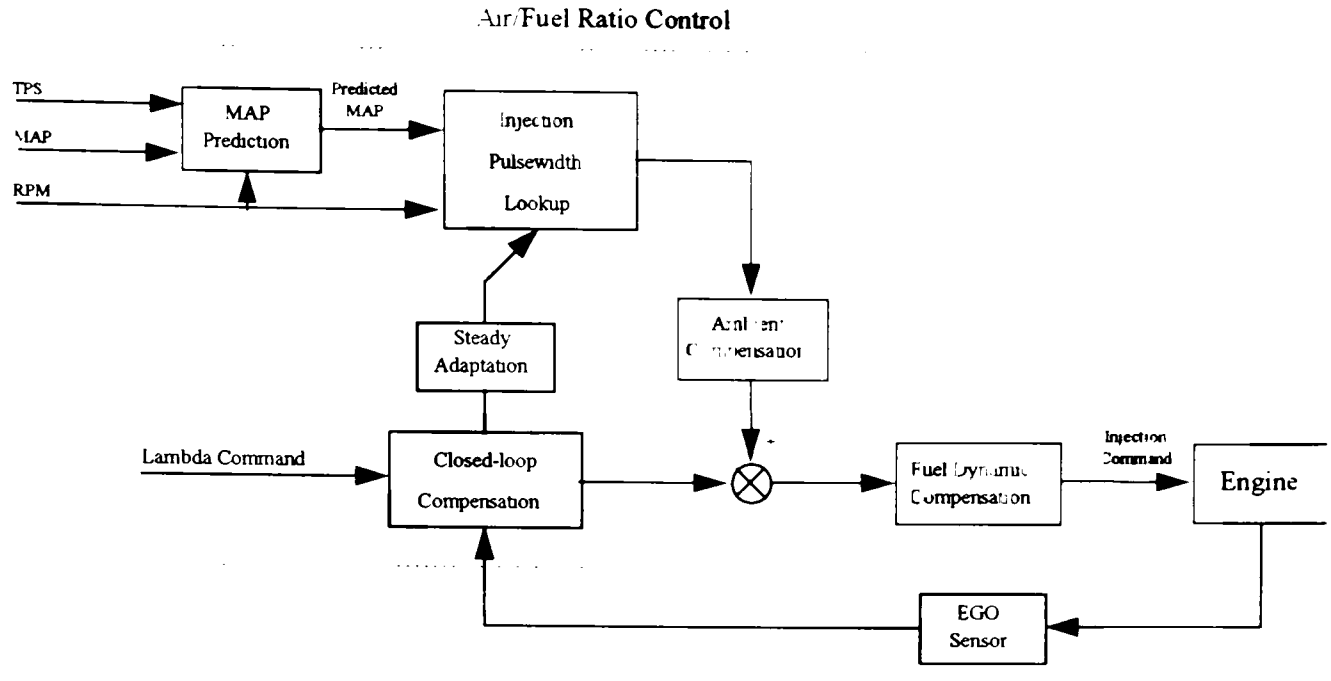

Figure 5.1 Full-featured Air/Fuel Control system

As shown in Chapter 2, the air charge, Am, can be determined by an instantaneous function of manifold absolute pressure (MAP) and engine speed (measured in Revolutions Per Minute [RPM]). In a real engine system, however, there are a few restrictions associated with this method, such as, dynamic lags and delays. First, the MAP sensor output is subject to cyclic oscillations induced by a manifold pumping effect. A low-pass filter is commonly used to eliminate these oscillations and obtain a mean-value for control calculation. This filter will inevitably introduce a lag in the air flow measurement [15]. Second, to allow time for injection pre-phase as well as fuel transport from the injector to the intake valve, the fuel calculation has to be made at two segments (360° crankshaft rotation) before the start of the corresponding intake event [15]. This introduces a pure delay in the injection command. These lags and delays, if uncompensated, can cause considerable air-fuel ratio excursion during engine transients. A MAP predictor can be used to solve this problem. The MAP predictor uses the throttle trajectory, which is accurate and instantaneous, to predict the MAP output two segments in the future.

The manifold filling phenomena can be described as [16]:

$$\dot{p}_{man} = \frac{RT}{V}[-\dot{m}_{ap}(n, p_{man}) + \dot{m}_{at}(\alpha, p_{man})] \tag{5.1}$$

where p_{man} is the manifold pressure, V is manifold volume, T is air charge temperature, $\dot{m}_{ap}(n, p_{man}) = \frac{V_d}{120RT} n\eta_{vol}(n, p_{man})p_{man}$ is the speed-density expression, and the air flow across the throttle $\dot{m}_{at}(\alpha, p_{man})$ is also an instantaneous function of throttle angle α and manifold pressure. This equation indicates a method of predicting the MAP based on the throttle angle history assuming that the throttle angle remains constant during the prediction period. Data fusion techniques, such as a Kalman filter, can be used to combine the MAP estimate given by this model with the actual MAP sensor output.

The second most important factor in the air/fuel system is the fuel dynamics, mainly the wall-wetting effect. A portion of the injected fuel will be deposited in liquid form along the walls of the intake system components. The buildup of a liquid puddle causes a lag in the amount of fuel actually drawn into the cylinders and results in an air/fuel excursion [15]. However this only happens to liquid fuels and does not apply to propane.

The 2-D injection pulse-width lookup table can provide for fast feed-forward control. Errors in the table, which may result from modeling error or changes in ambient or engine conditions, can be compensated for by the O_2S sensor feedback control during steady-state engine operation. However, O_2S feedback control is too slow to be able to correct the error promptly during fast engine transients. The errors in the table can again

cause air/fuel excursion during a fast transient. Steady-state adaptation ensures that the data in the table are continuously adjusted toward the elimination of those errors.

A full implementation of the air/fuel control system requires a large amount of development effort and engine modeling. Due to time and equipment constraints, only part of the blocks given in Figure 5.1 are currently implemented in the TTUCM. Figure 5.2 shows the block diagram of the TTUCM air/fuel control.

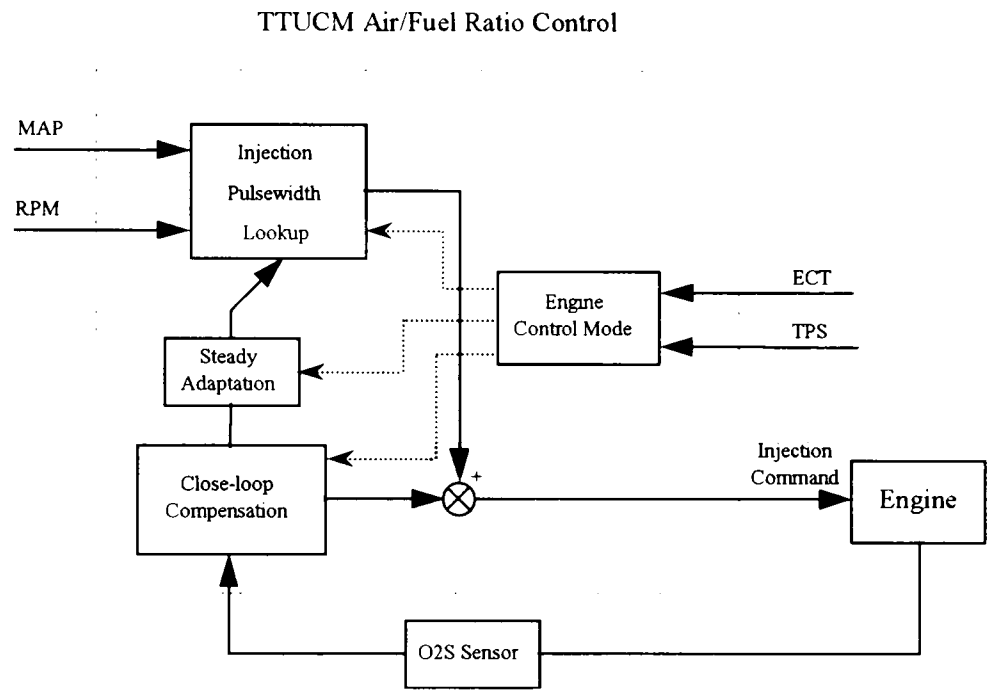

Figure 5.2 TTUCM Air/Fuel Ratio Control Block Diagram

The software for air/fuel ratio control was developed in three stages: setup of the initial fuel map, open-loop control and closed-loop learning control. This corresponds to the three components of the final control software: control data, low-level control and high-level control. The three stages are discussed separately in the following sections with emphasis on the corresponding component developed in each stage.

5.2.2 Setup of Initial Fuel Map

5.2.2.1 Introduction

The engine air/fuel system is a highly nonlinear system. Most control algorithms work around operating points. The implication is that the engine must be running while the control algorithms can fine-tune the air/fuel ratio and provide for dynamic compensation. The first step in engine control is therefore to set up a fuel map that defines the basic fuel requirement under all engine operation conditions.

The air charge, Am, was shown in Chapter 2 to be an instantaneous function of MAP and engine speed. The fuel map for stoichiometric air/fuel ratio control is thus a two-dimensional table referenced by the MAP and engine speed. Stored in each table location is the amount of fuel to be delivered for stoichiometric air/fuel ratio. In the case of a fuel injection system, the fuel amount may be represented by the fuel injection pulse-width, assuming that the fuel pressure is repeatable.

A number of methods exist for the setup of the fuel map. Most after-market conversion kits use theoretical calculations in combination with a Universal Exhaust Gas Sensor (UEGO)-aided manual fine-tuning, which proves to be quite time-consuming and costly. An automatic fuel map setup method was used instead in this project. With adaptive learning capabilities, the in-stock PCM can, to a certain degree, adjust its own fuel map to accommodate for the changes in fuel characteristics and system configuration as long as it can get into closed-loop operation. A program was developed to record the PCM injection pulse-widths while the engine went through all the operation conditions. The recorded injection pulse-widths are believed to be close to what are required for the

stoichiometric ratio after the PCM gets sufficient training and is able to get into closed-loop operation. A fuel map can then be set up based on this recorded data. This fuel map can be used for basic open-loop engine control, as well as the study of engine characteristics and the PCM control strategy. This method does not require a priori knowledge of engine specifications and air intake system model. It is fast and can be readily ported to other engine systems.

The initial fuel map doesn't have to be very accurate. The basic requirement is just to make engine run stablely under all operating conditions when this map is later used in open-loop control. The elimination of error in the map is to be done later by the closed-loop learning control.

5.2.2.2 Design and Implementation

The TTUCM hardware is set up as follows. The conditioned crankshaft position signal is connected to TPU channel 0 for engine speed measurement, and the conditioned MAP signal is connected to ADC AN0. The PCM injection signal is tapped off to a clamping circuit before being input to a spare Isolation Digital channel on the interface board. The output of the channel is then connected to TPU1.

The TPU time function Period/Pulse-width Accumulator (PPWA) is used to measure the engine speed and the PCM injection pulse-width. The PPWA function allows any channel of the TPU to accumulate a 24-bit sum of either the period or the pulse width of an input signal over a number of periods programmable from one to 255 periods or pulses [10]. TPU1 works in the PPWA pulse mode in which the width of only one

injection pulse is measured each time. TPU0 works in the PPWA period mode in which the periods of eight crankshaft pulses are accumulated. By examining the crankshaft pulse pattern in Figure 3.1, it is seen that the period of eight crankshaft pulses amounts to 2/3 engine revolution independent of the phase difference between the TPU and the cylinder position. So this approach does not require engine signal synchronization.

The program basically consists of two interrupt service routines (ISR). One interrupt is generated by TPU0 PPWA. The ISR stores the current measurements of 2/3 engine period and the MAP in the memory and reinitialize the TPU0 for next period measurement. The other interrupt is generated by TPU1 PPWA. The ISR fetches the measurement of the latest injection pulse-width from TPU1 and stores it in the table location determined by the current MAP and 2/3 engine period, and then reinitializes the TPU1 for the next injection pulse-width measurement.

The generated fuel map is defined as follows. A table element is referenced by two engine state variables: MAP and 2/3 engine period. The 0~5V MAP sensor output stretches 64 linear scales, and results in a resolution of 5/64 = 0.078 V The resolution of 2/3 engine period is 1.024ms. Its range, 6.144 ~ 80.896 ms, which corresponds to 494 ~ 6510 RPM, is covered in 73 linear scales. The resulting table dimension is 64 by 73. Each table element is a 16-bit unsigned integer. The actual injection pulse-width can be determined by table data multiplied by 8 us.

5.2.2.3 Experimental Result

Experiments were conducted using the program discussed above to obtain a series of fuel maps under various operating conditions.

5.2.2.3.1 Closed-loop Fuel Map Experiments. Engine configuration was as follows: Bosch compressed natural gas (CNG) fuel injectors, 120 psi (pounds per square inch) fuel vapor pressure, EGR disconnected to eliminate its interference with the MAP measurement. The PCM was given extensive training in mid-temperature range the day before the experiment. Before the actual data acquisition, the engine was warmed up to mid-temperature and operating in closed-loop mode. The Minivan was put on a chassis dynamometer and driven through the full range of load and speed while the PCM injection pulse-width was continuously recorded.

Figure 5.4 and Figure 5.3 plot the recorded injection pulse-width data and its distribution. The Minivan was driven under broad operating conditions during the test, however due to the limitations of the dynamometer, there were still some unreached conditions, which appear as holes in Figure 5.3. The injection pulse-width surface is generally smooth in Figure 5.4. The discontinuity in the left/up corner, which corresponds to the high speed and high load operation, is due to WOT operation. In the WOT mode, the PCM operates in open-loop and enriches the air/fuel ratio to around 0.9 to obtain maximum power output. The surface reveals the non-linearity of the air intake system.

The experimental results are believed to be consistent and reliable. Comparison is given between the data from two separate tests conducted three days apart. As shown in Figure 5.5, the difference is small except for at some points in the WOT region, which can

be explained by the assumption that the PCM might not have recognized the WOT condition at some points during one of the tests.

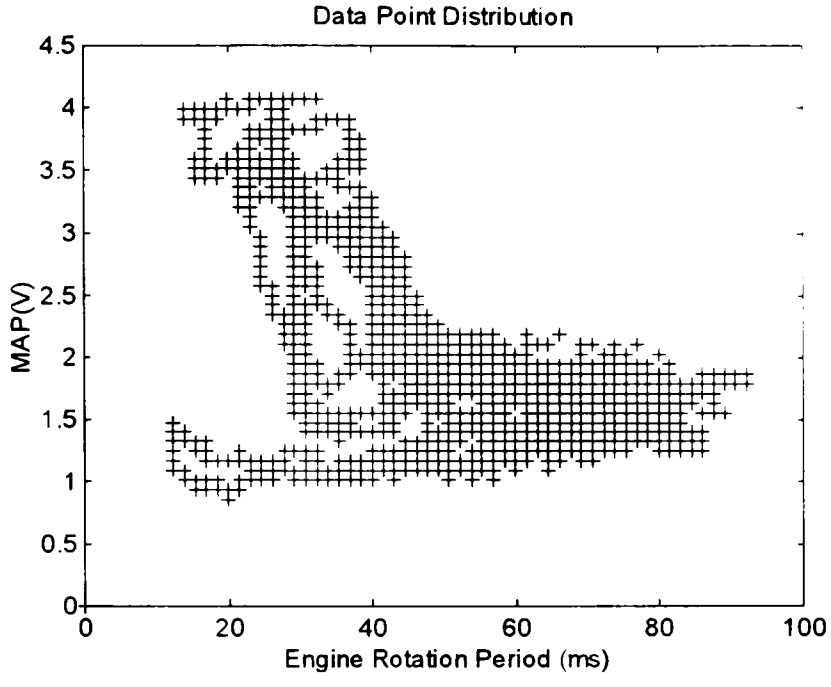

Figure 5.3 Injection Pulse-width Data Distribution

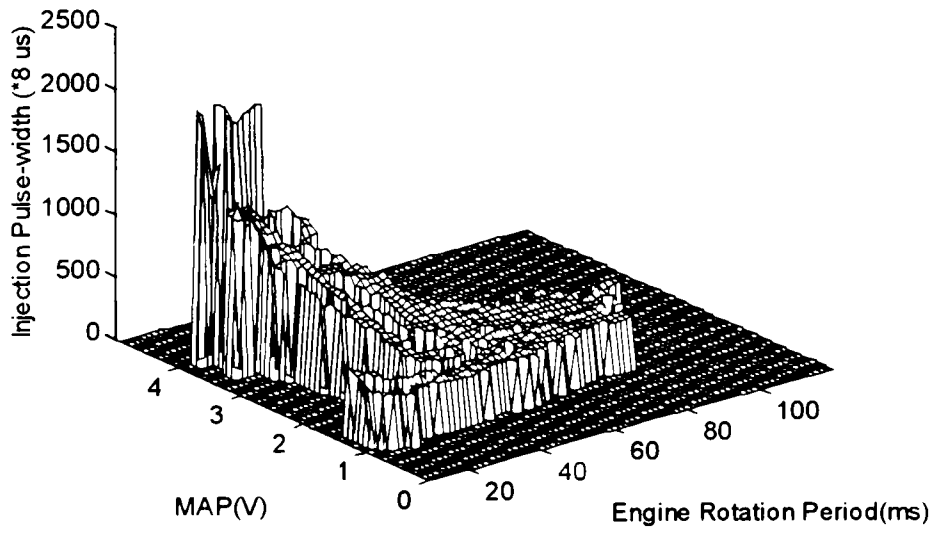

Figure 5.4 Closed-loop Fuel Map

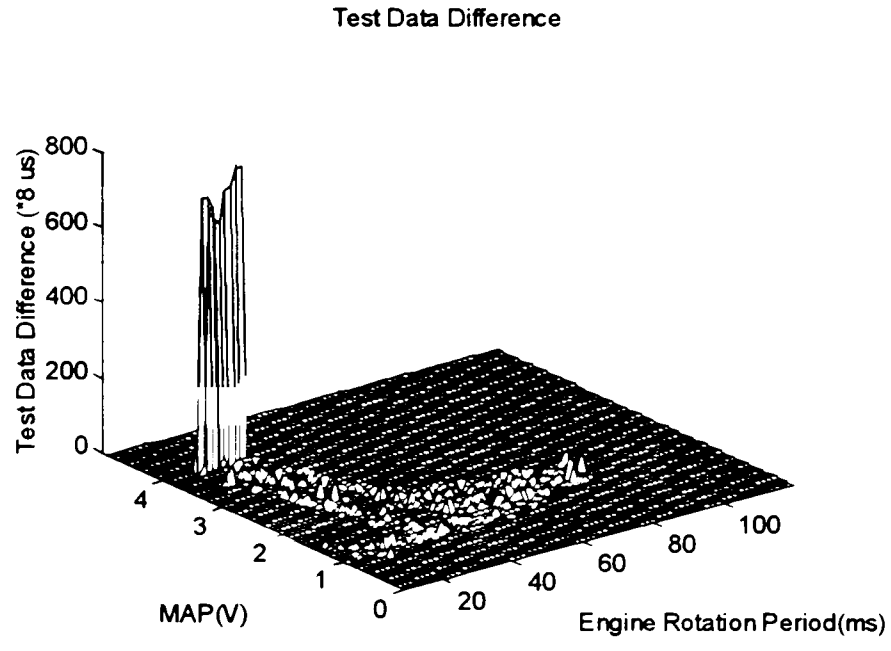

Figure 5.5 Test Data Difference

5.2.2.3.2 Open-loop Fuel Map Experiment. The engine configuration remained the same. The battery was disconnected before the experiment to reset the fuel maps stored in the PCM RAM. Both upstream and downstream O_2S sensors were disconnected to block the PCM learning during the test. The fuel maps recorded in this way are believed to be the base PCM fuel maps. In the first test, the ECT input to PCM was set at 2.24 V through a variable resistor acting as a dummy ECT sensor, and the dash temperature gauge reading was "cold." The recorded PCM injection pulse-width is plotted in Figure 5.6. In the second test, the ECT input was set at 2.25 V, and the dash temperature gauge reading was "medium warm." Figure 5.7 shows the PCM injection pulse-width recorded in this test.

Two groups of data are compared in Figure 5.8. The injection pulse-widths with cold engine can be seen to be approximately 20% longer than with warm engine. That is supposed to be the PCM's cold enrichment coefficient for gasoline. Propane, which is in

vapor phase at room temperature and atmosphere pressure, should require a cold enrichment coefficient less than 20%.

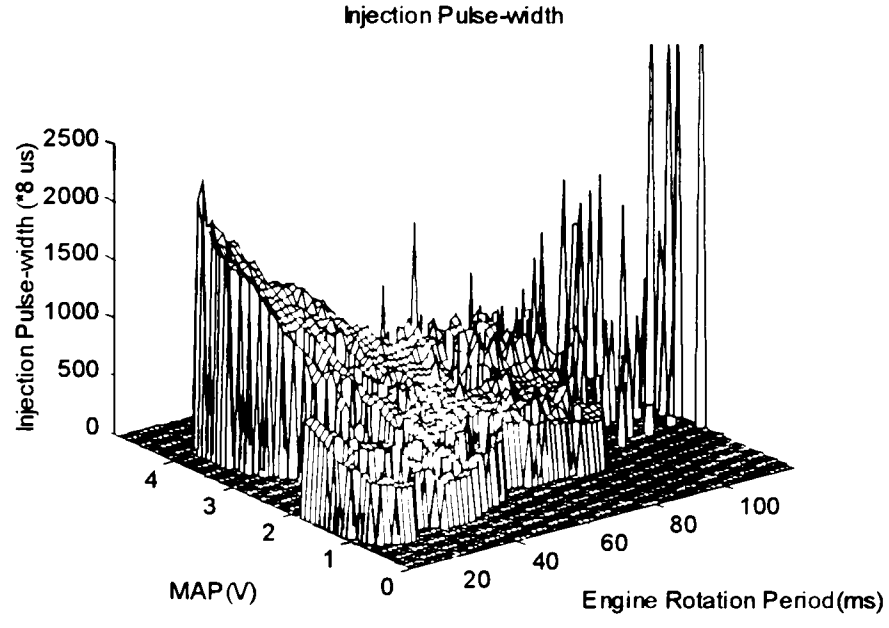

Figure 5.6 Open-loop Fuel Map with Cold Engine

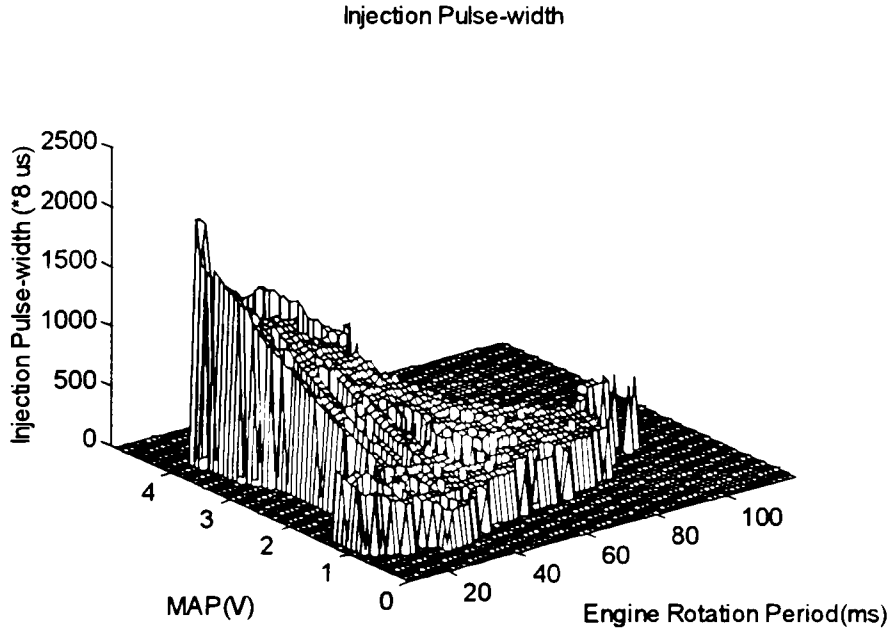

Figure 5.7 Open-loop Fuel Map with Warm Engine

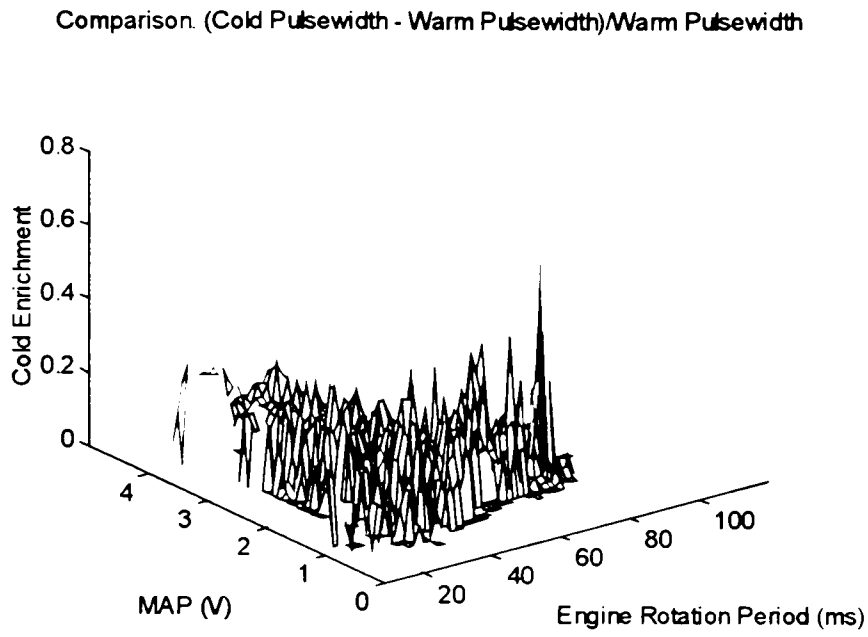

Figure 5.8 Cold Enrichment

5.2.3 Open-loop Control

5.2.3.1 Introduction

After the initial fuel map was obtained, the second experiment was conducted to control the engine air/fuel ratio in open-loop mode. In this experiment, the TTUCM controller took over the engine air/fuel ratio regulation by controlling the fuel injection while leaving the PCM to control the rest of the system. The TTUCM controller derived its fuel injection command directly from the fuel map obtained in the first experiment. The O_2S sensor feedback was ignored.

The objective of this experiment was to make the engine run stablely under the TTUCM's open-loop control of air/fuel ratio. The tasks included the implementation of the low-level timing controls, and the setup of the basic software structure into which future developments on advanced control algorithm can be incorporated. Also tested were the functionality of the TTUCM controller hardware as well as its wiring with the

engine system. The PCM was for the first time partially bypassed. Observations were made on its reactions.

The main problems addressed in this experiment were the engine signal synchronization and the injection timing control. Direct electronic controls of spark ignition and sequential injection call for the synchronization of the control events with engine cylinder position. A good synchronization scheme should have the capabilities of maintaining the synchronization robustly, prompt detection of the loss-of-synchronization caused by spurious synchronization signals or position sensor defects, safe out-of-synchronization operations, quick and reliable lock-in from the start-up or loss-of-synchronization, along with low CPU overhead. Accurate injection timing control lends much to the sequential injection's advantage over other fuel metering schemes. The TTUCM control software adopts a simple sequential injection timing control scheme, and still the effects of some injection timing control parameters were observed in the experiment.

The software developed in this experiment was reused in the subsequent software development when new modules were added onto it. Emphasis was given in the design to providing a reliable and encapsulated low-level implementation for the basic control algorithm.

5.2.3.2 Design and Implementation

The TTUCM air/fuel control software is defined as a three-layer structure, as illustrated in Figure 5.9.

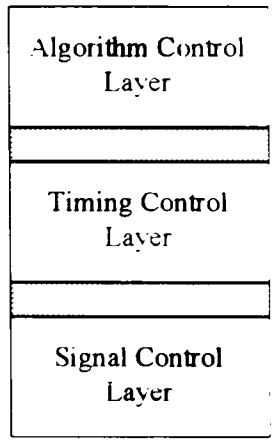

Figure 5.9 TTUCM Air/fuel Control Software Structure

On the bottom is the signal control layer which directly interacts with engine sensor signals as well as gives actuator control signals, and treats them as level signals. This layer is mainly implemented by the microcoded TPU time functions and ADC conversion sequence control hardware. The signal control layer communicates with the timing control layer through the host interfaces of ADC and TPU time functions, which include a group of system configuration registers, channel control/status registers and channel parameter registers.

The timing control layer implements the control commands from the algorithm layer by coordinating the activities in the signal control layer. It conceals the detailed low-level operations and provides a simple algorithmic interface to the upper layer. Its interface to the algorithm control layer consists of a group of shared measurement/control variables, status flags and event-scheduling interfaces.

On the top is the algorithm control layer. A high-level control algorithm is implemented in this layer. Depending on the computational complexity of the algorithm, assembly or a high-level language can be chosen as the programming language for this layer.

The three layers are functionally isolated from each other and communicate through well-defined interfaces. Changes in the implementation of one layer should not affect the other layers.

In the open-loop experiment, a synchronization and timing module was developed to implement the timing control layer. This module remained unchanged as a component in the subsequent software. The algorithm control layer was implemented by a simple open-loop control module, which was later replaced by the closed-loop learning control module in the final software.

5.2.3.2.1 Synchronization and Timing Control Module. The synchronization and timing control module synchronizes the control events with the engine cylinder position and implements the injection command given by the algorithm layer. Its interface to the algorithm layer is defined in Table 5.1.

Table 5.1 Timing-Algorithm Layer Interface

Interface Name	Interface Definition	Data Flow
MAP	Filtered MAP measurement	Timing → Algorithm
PER24	240° Crank angle period	Timing → Algorithm
INJPW	Commanded Injection pulse-width	Algorithm → Timing
MINF	Validity flag of current measurement	Timing → Algorithm
LOCKF	Synchronization status flag	Timing → Algorithm
CRKC	Event-based Call Entry	N/A
CTLINT	Time-based Call Entry	N/A

Two calling interfaces are included: time-based and event-based. The time-based call is scheduled at constant-time intervals, while the event-based call is synchronous with the crank-angle. The event-based control is justified by the discrete nature of the engine

operation, where physical processes are naturally divided into four distinct regimes corresponding to the four engine events: intake, compression, power and exhaust. Most dynamics vary less in the crank angle domain than in the time domain [17]. Event-based control can simplify the design in most cases.

Four TPU time functions are used: Period measurement with missing transition detection (PMM), Position-synchronized pulse generator (PSP), Input capture/input transition counter (ITC), and Output compare (OC). PMM enables special-purpose period measurement between normal input transitions for a channel that has its input connected to the same source as the input to an internal counter, TCR2. The PMM detects the occurrence of a missing transition as indicated by the current period measurement being more than a programmable ratio times the previous period measurement. Once detected, this condition can be counted and compared to a programmable number of transitions that are to be detected before TCR2 is reset to $FFFF Also, the nonzero value of a flag can cause TCR2 reset. This function, used on the crankshaft position signal, effectively maps engine-cycle position to TCR2 count [10].

The PSP can generate an output transition or pulse, which is a projection in time based on a reference period previously calculated on another channel [10]. In this application, the PSP is used to generate the injection pulses. The reference period is the engine cycle period derived from the crankshaft pulse period measured using the PMM. Both the widths and trailing edges of the injection pulses can be accurately controlled.

The ITC can count a programmable number of transitions and capture the specified timer upon the occurrence of the final transition [10]. It is used in junction with

the PMM for engine cylinder position signal synchronization. The OC can generate a specified edge at a programmable delay time from a user-specified time. It is used to generate injection pulses during out-of-synchronization operation.

The crankshaft position signal is connected to the TCR2 and two TPU channels, running PMM and ITC respectively. The camshaft position signal is connected to another channel running ITC. Six TPU channels running PSP generate control signals for six injectors. Two distinct modes exist in the operation of the timing control module: in-lock and out-of-lock. They are briefly described, as follows, by referring to Figure 5.10.

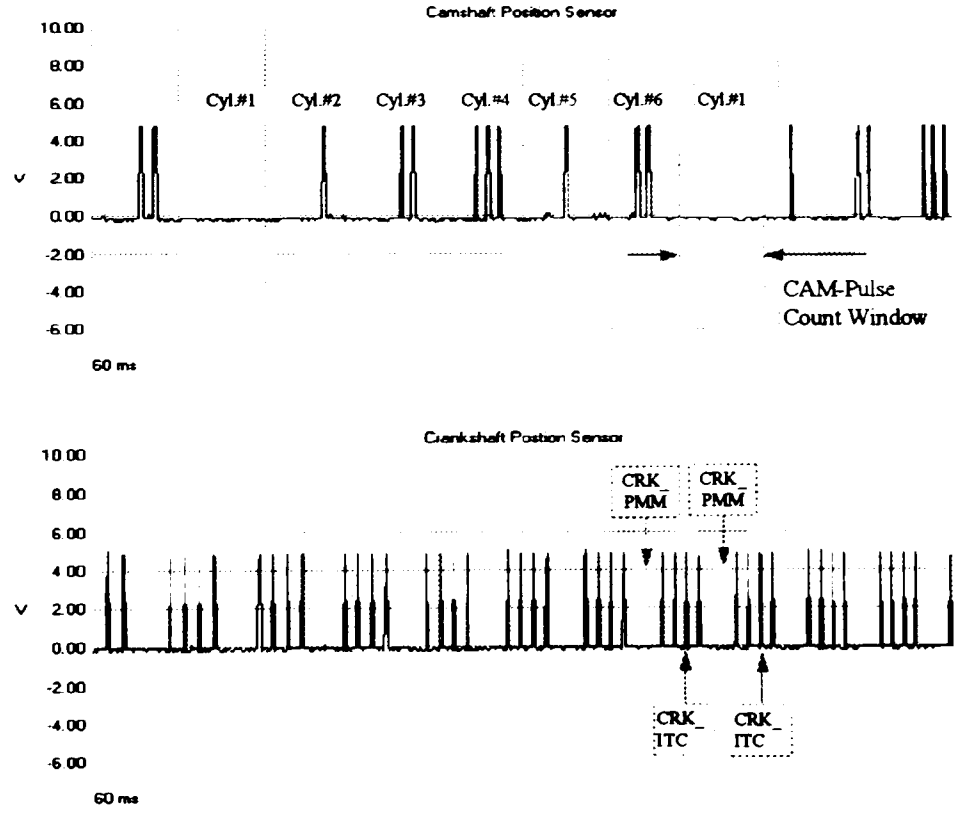

Figure 5.10 Engine Position Signal Synchronization

In the in-lock mode, synchronization is maintained. The PMM detects the transition missing between two groups of crankshaft pulses and generates an interrupt to the CPU. The ISR (CRK_PMM) checks if the synchronization is maintained, updates certain parameters to sustain the synchronization, and starts the crankshaft ITC to delay

for 3 crankshaft pulses. The control parameters of the corresponding injection control channel are also updated based on the current command given by the algorithm module. Another interrupt is generated after the crankshaft ITC counts 3 pulses. Its ISR (CRK_ITC) then initializes the camshaft ITC for the pulse count if the current cylinder number is 6; or fetches from the camshaft ITC the pulse count since last CRK_ITC (cylinder #6) if the current cylinder number is 1. This camshaft pulse count provides the cylinder sequence confirmation. Only six CRK_PMM and CRK_ITC interrupts are generated every engine cycle.

A simple injection timing control scheme was used in the timing control module. The end of injection is fixed at 180° crank-angle prior to the close of the intake valve while the beginning of the injection is moved forward as required to allow for enough time for the fuel injection process. Advance of less than 150° was assumed to be insufficient for the fuel to travel to the intake valve, and was observed to cause rugged idle operation.

The timing module operates in an out-of-lock mode upon start-up or after detecting loss of synchronization. The CRK_PMM and CRK_ITC work in a similar fashion as the in-lock mode, except that CRK_ITC always fetches the CAM_ITC count and reinitializes CAM_ITC for next count. The CRK_PMM needs to handle the PMM error properly and watch for the passing of cylinder#1, upon which the synchronization is regained. A simultaneous injection scheme is used in out-of-lock operation.

More details can be found in the flow chart of the timing control module given in Figure 5.11.

5.2.3.2.2 Open-loop Control Module. The open-loop control module is time-based and scheduled every 20 ms. It reads the MAP and PER24 measurements provided by the timing control module, finds the corresponding injection pulse-width in the fuel map, and scales it before writing into the INJPW.

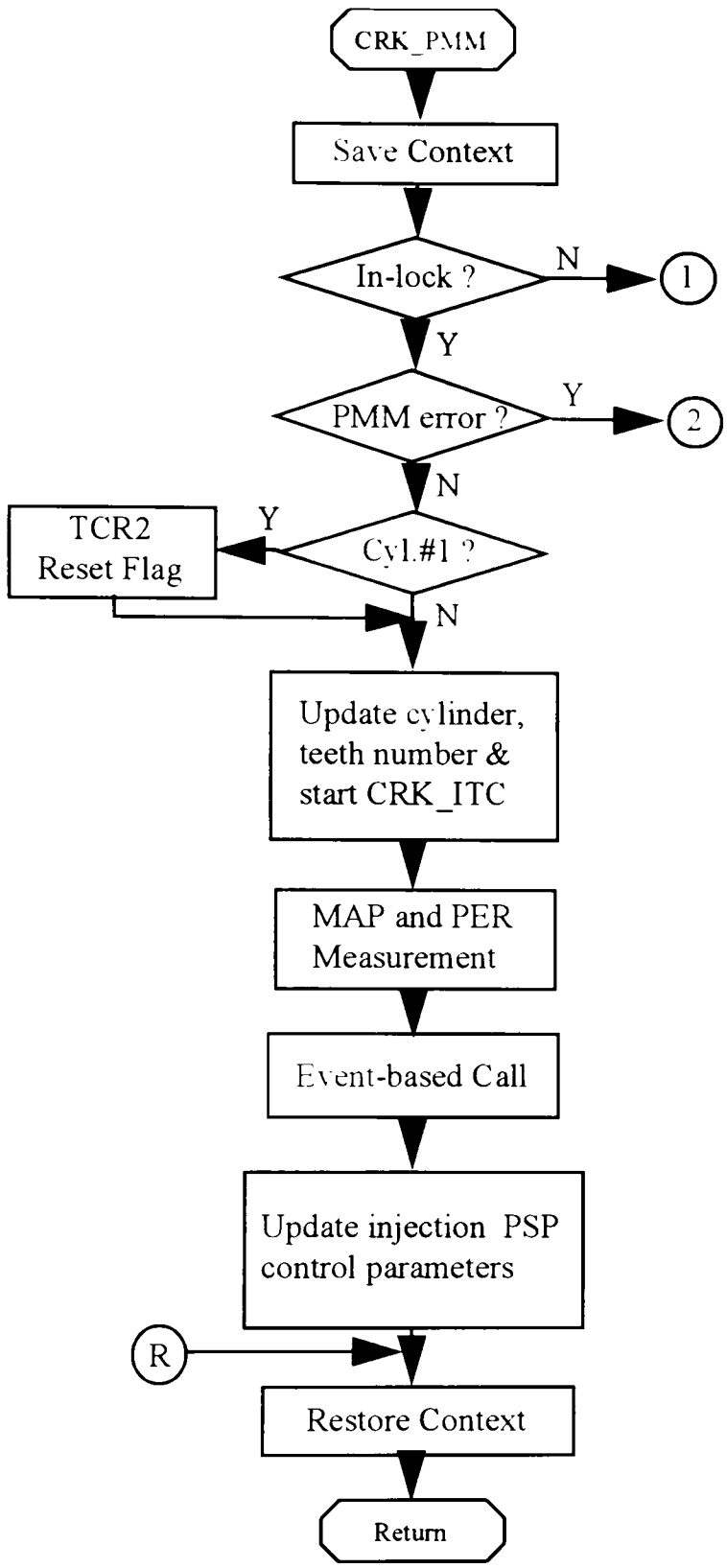

Timing Control State Diagram

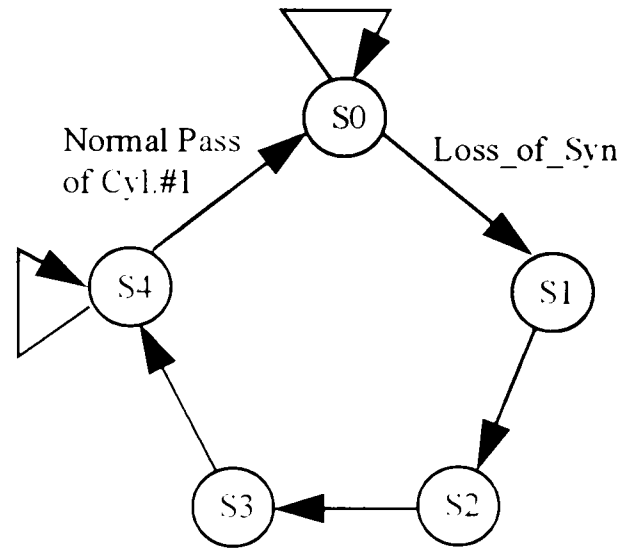

Note:

1. The clock-tick in the above state diagram is every execution of the CRK_PMM
2. The state number corresponds to the LOCKF value.
3. S0 . In-lock; S1-S4. Out-of-lock

Figure 5 11 Timing Control Module Flow Chart

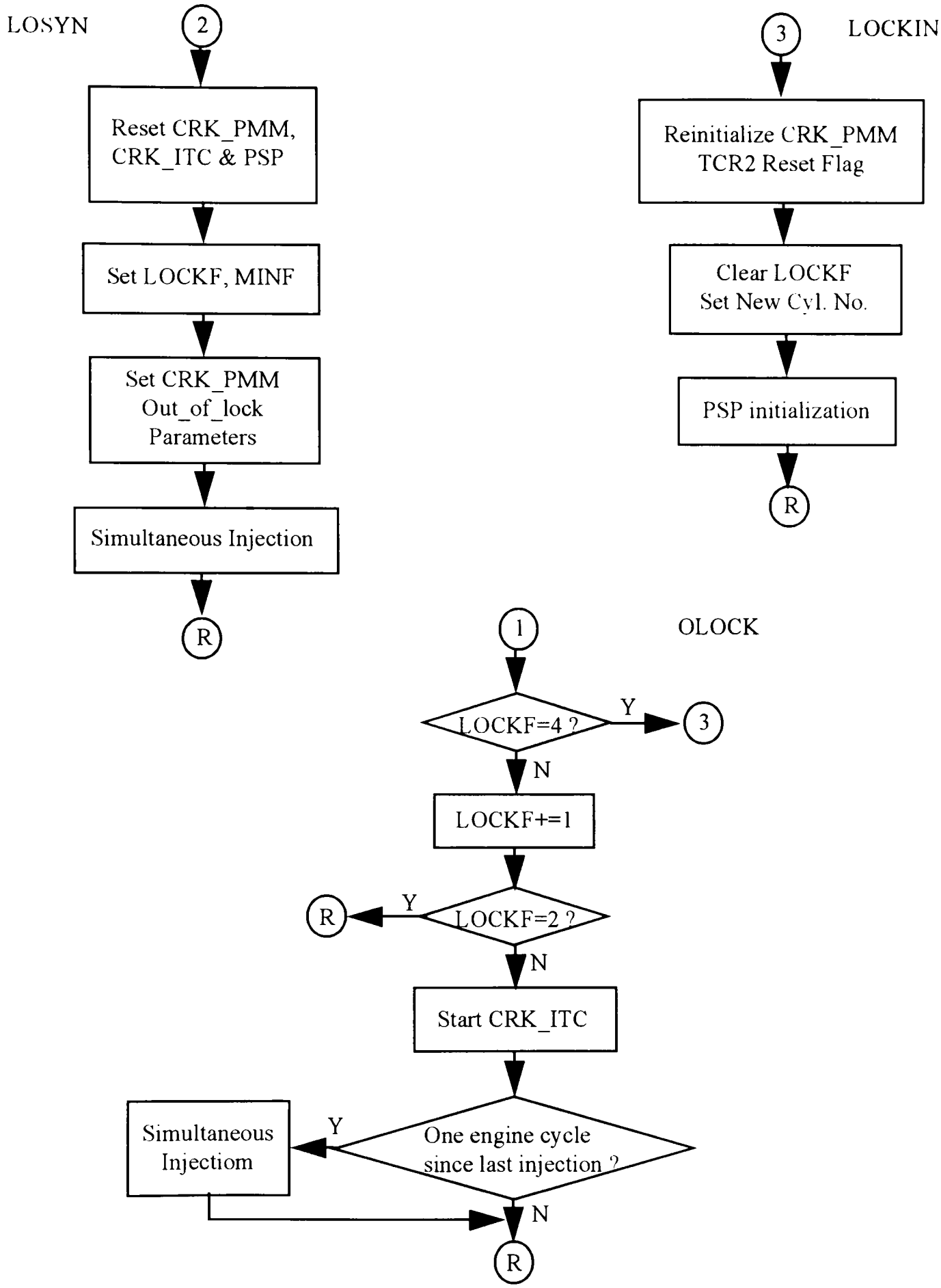

Figure 5.11 (continued)

5.2.3.3 Experimental Result

Engine configurations for this experiment: Bosch CNG injector, 120 psi fuel vapor pressure, up/down stream O_2S sensors disconnected, EGR disabled. The control fuel map, as shown in Figure 5.12, was derived from the initial fuel map obtained in the first experiment by interpolation and exptrapolation in the unreached areas. The engine could run stablely under all operating conditions with a scaling factor of 1.1. The PCM, as expected, only indicated the malfunction of O_2S sensors and EGR.

The timing control module manifested very robust performance. No loss-of-synchronization, loss or addition of injection pulses were observed during transient. The engine even could sustain operation during a quick hardware reset-and-release at idle.

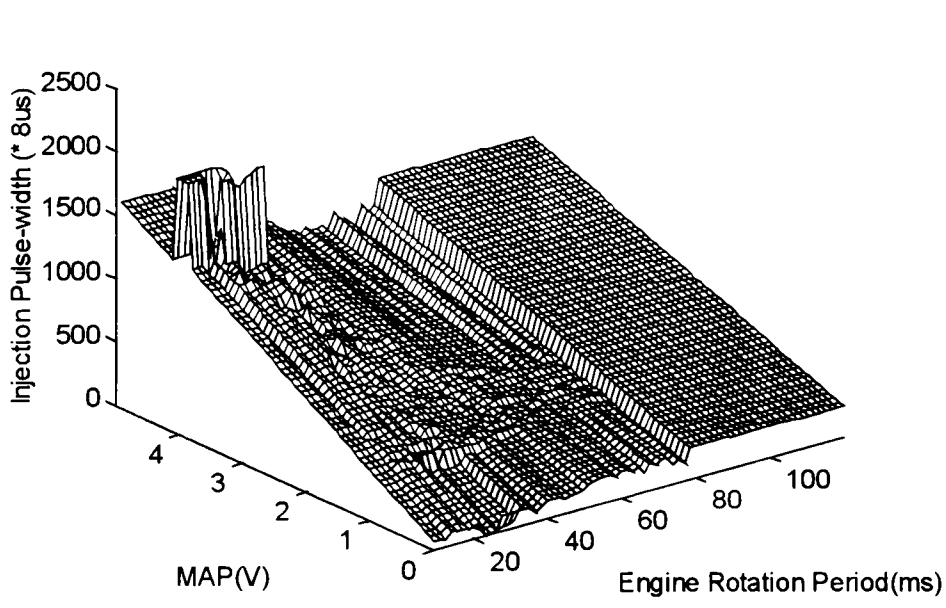

Figure 5.12 Derived Fuel Map

5.2.4 Closed-loop Learning Control

5.2.4.1 Introduction

In the third stage, closed-loop learning control was introduced to more accurately control the air/fuel ratio. The control strategy consists of three components: closed-loop PI control, anticipatory feed-forward control and learning control.

Incorporating the O_2S sensor feedback in the actual air/fuel ratio, closed-loop PI control provides short-term compensation for the steady-state error in air/fuel ratio, which may be caused by the errors in the initial fuel map, changes in environmental conditions, engine aging or other unmodeled effects. However, the closed-loop PI control alone has the disadvantage of slowing down the system response during fast transients. Based on the open-loop control developed in the last experiment, the anticipatory feed-forward control overrides the closed-loop control during fast transients by reinitializing the injection pulse-width to the stored table value corresponding to the new engine operating point, and thus significantly increases the system bandwidth. The learning control adapts the fuel map using the experience gained in the closed-loop control and thus indirectly improves the accuracy of the anticipatory feed-forward control. It provides a mid-term compensation for slow-varying errors.

The three components address different aspects of the control problem. In terms of response time, anticipatory feed-forward is fastest with closed-loop PI control the next and learning control the slowest. The three components were coordinated to provide improved air/fuel control accuracy over short-term as well as long-term.

The synchronization and timing control module was reused to implement the timing control layer while new software was developed exclusively in the algorithm layer. Due to the low computational complexity of the algorithm, assembly language was used as programming language.

5.2.4.2 Algorithm Design

5.2.4.2.1 Closed-loop PI Control. Closed-loop air/fuel ratio control adjusts the fuel command based on the air/fuel ratio feedback from the O_2S sensor. Research in recent years has been focused on the application of advanced control techniques, such as state-space method, Kalman filter and adaptive control, and several successful attempts have been reported [15, 17, 23]. Most of this research assumes the availability of a Universal Exhaust Oxygen Gas sensor (UEGO), which is much more linear around the stoichiometric region and is expensive. Due to cost consideration, however, a less expensive switch-type λ sensor is commonly used in most if not all, of production engines.

Simulations were run to compare the performances of Kalman filter-based control and conventional PI control on both UEGO and λ sensor systems. Figure 5.13 shows the block diagram of the Kalman filter-based (KF) controller. This controller was modified from the one proposed in [17]. Its core is a constant-gain discrete Kalman filter which estimates the fuel command error based on the O_2S sensor output. The Injection PW Control unit then adjusts its command to offset this error. An exhaust-sensor path model is embedded in the KF controller.

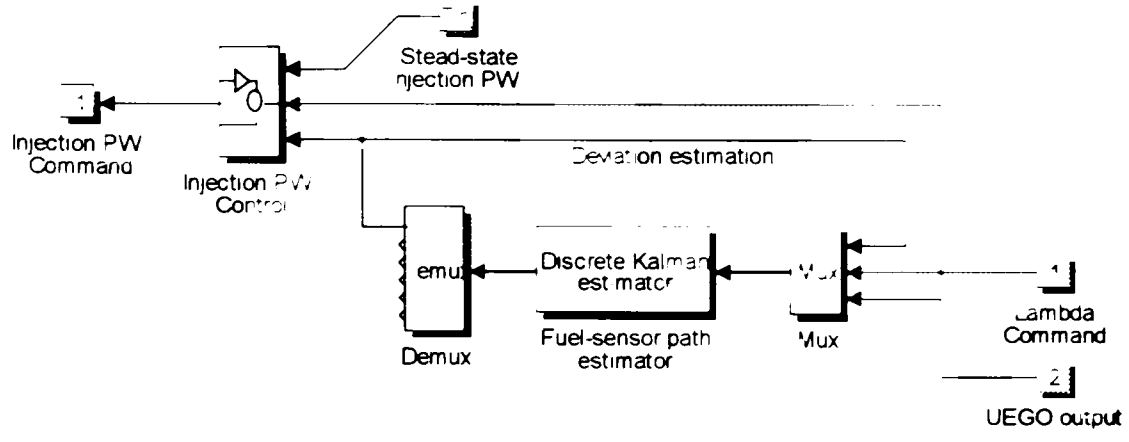

Figure 5.13 Kalman Filter-based Control

In Figure 5.14, the performances of the optimal KF control and PI control are compared, on an UEGO system under an 11% constant disturbance which can alternatively be interpreted as an initial fuel command error. Both the UEGO time constant and the exhaust transport delay are assumed to be 120ms. It is obvious that the KF control can provide much faster compensation for the steady-state error than the conventional PI control. Further simulations also indicate that the KF control is more robust than PI control. However, with the λ sensor system, the two control strategies give comparable performances as shown in Figure 5.15, and sometimes the Kalman filter control can be even worse. This might be explained by the fact that the advantage of Kalman filter, which is built on the knowledge of plant model, diminishes with the scarcity of feedback information. PI control was thus chosen for the closed-loop air/fuel control considering its simplicity and robustness when used with a λ sensor system.

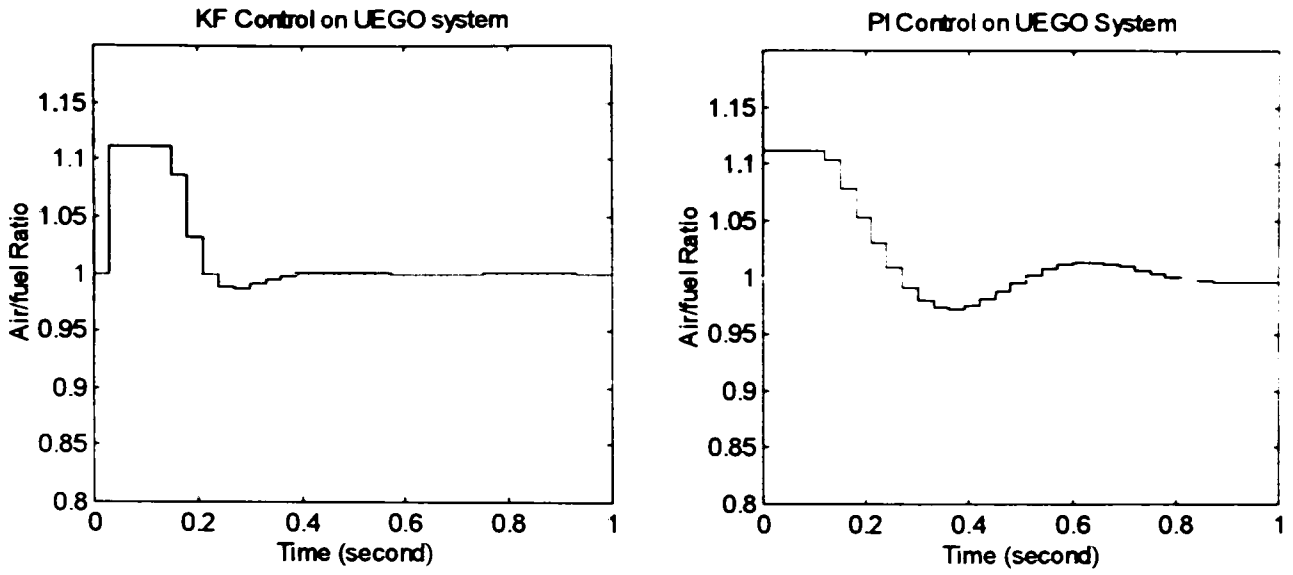

Figure 5.14 Optimal KF and PI Control on UEGO System

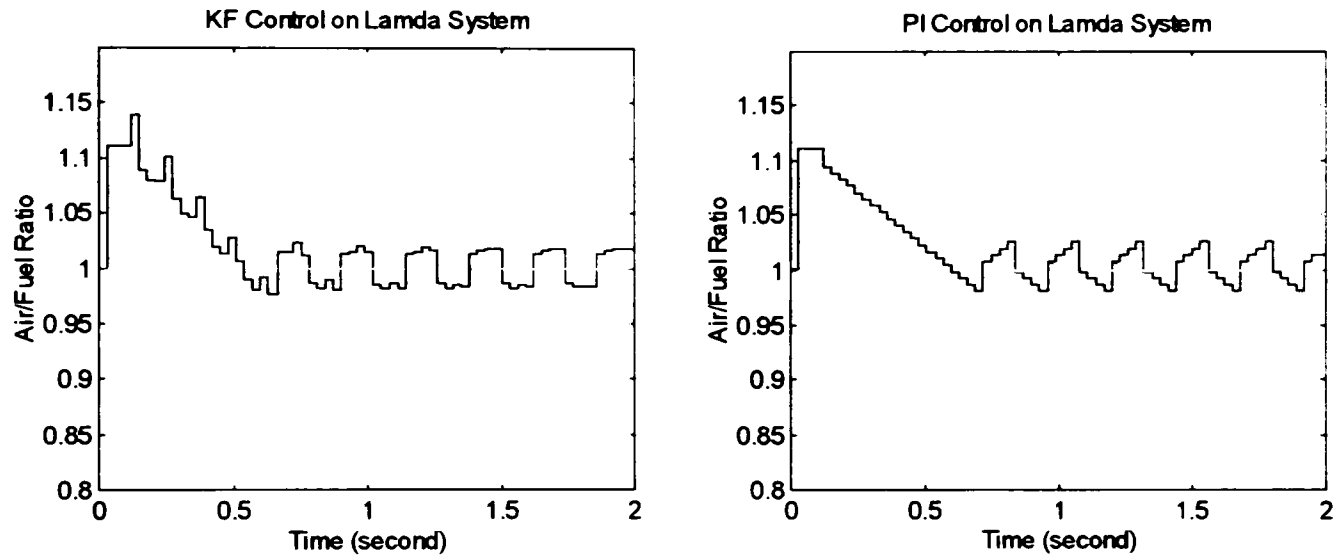

Figure 5.15 KF and PI Control on Lamda System

The O_2S sensor output $\phi_m(k)$ is processed through a comparator and converted into a switch signal, and the PI control can be formulated as

$$\phi_{sw}(k) = \begin{cases} +1 & \text{if } \phi_m(k) > \text{Bias} \\ -1 & \text{if } \phi_{m(k)} \le \text{Bias} \end{cases}$$

$$u(k) = u(0) - Kp * \phi_{sw}(k) - Ki * \sum \phi_{sw}(k). \qquad (5.2)$$

The proportional gain Kp and integral gain Ki can be calibrated under different operating conditions and stored in a gain-schedule table to obtain a global optimal

performance. Due to the time constrains, only constant Ki and Kp were used in the experiment. The u(0) is the initial value of the PI integrator.

A limit-cycle behavior exists in the O_2S sensor output under closed-loop control. Limit-cycle is an oscillation in the output of the system that possesses delay and switch-type components in the control loop. The steady-state oscillation frequency and amplitude are given by

$$f_l = \frac{1}{4Td} \qquad A_l = \frac{Ki * Td}{Ts} \tag{5.3}$$

where Td is the total delay in the control loop, and Ts is the sampling period. Since Td varies with the engine speed and is more constant in the crank-angle domain, the closed-loop PI control used here is event-based instead of conventional time-based. Due to the storage and average effects of the catalyst converter, the resulting oscillation in the air/fuel ratio can actually help to broaden the high-efficiency conversion window to about ±3% [17].

5.2.4.2.2 Anticipatory Feed-forward Control. The anticipatory feed-forward control ignores the O_2S sensor feedback and bases the decision completely on the available engine state variables: MAP and PER24. The algorithm consists of two parts: Fast transient criteria and Operating point reinitialization. Both of them have significant effects on the stability of the engine operation as well as the efficiency of the learning control, especially at low engine speed.

The engine states are continuously monitored. When the change in the engine states is found to be rapid enough to meet the Fast transient criteria, the control is quickly

reinitialized to the new operating point (Jump operation). Otherwise only the continuous closed-loop PI control takes charge (Crawl operation).

A change in the engine operating point is regarded as a fast transient if one of the following conditions is met.

1. The MAP output changes more than MAPJ1S (constant) within one sample period;
2. The MAP output changes monotonically in two consecutive sample periods and the total change is more than MAPJ2S (constant);
3. The PER24 changes more than PJ1S (constant) within one sample period;
4. The PER24 changes monotonically in two consecutive sample periods and the total change is more than PJ2S (constant).

The Operating point reinitializaion (Jump operation) includes the following steps:

1. Reset the jump timer to zero;
2. Reset the PI integrator (u(0) in equation 5.2), fuel command INJPW and the learning unit to the stored table value corresponding to the new engine operating point.

5.2.4.2.3 Learning Control. Every time a fast transient happens, the PI integrator and the fuel command INJPW will be reset to the stored table value corresponding to the new engine operating point. The error in this value will later be compensated for by the PI integral process. Before this integral process completes, however, the air/fuel ratio will deviate from the stoichiometric point. The learning control uses the most recent fuel injection command, which has being fine-tuned by the PI control, to update the fuel map.

Several factors will affect the learning speed and learning accuracy of the fuel map. In general, these factors include the map grid size, the frequency, magnitude and region of

the map update [18][19]. A simple approach, which serves the purpose of providing fast air/fuel control, is to compute a low- passed version of the fuel command u(k) [17].

$$W(k) = (1-\alpha)W(k-1) + \alpha u(k) \qquad (5.4)$$

The learning unit, W(k), will be used to update the fuel map right before the engine operating point slips out of one fuel map location and into another one. Upon the detection of a fast transient, W(k), will be reset to the stored table value for the new engine operating point so that subsequent learning will be based on the appropriate initial value. The filter constant, α, is chosen as a trade-off between learning speed and learning accuracy. It basically determines how long the engine should stay in a particular operating point such that W(k) can be completely updated to a new value. α was set at 0.125 during the experiment.

5.2.4.2.4 Modifications to Improve the Idle Operation. The algorithms introduced so far worked satisfactorily at engine speeds over 1000 RPM. However, at low engine speed, especially during idle, the closed-loop control induced considerable RPM fluctuations as it tried to decrease the fuel injection pulse-width to achieve the stoichiometric. With such an unstable operation, the learning control also became very inefficient.

Two assumptions were proposed for the explanation of the situation. First, the fuel injector delivered so high a flow rate to the point that it became almost uncontrollable in its meaningful range for this application. Before the third experiment was conducted, the Bosch CNG injectors were replaced by high flow-rate BKM SP-14 injectors as a solution to the low fuel pressure cold start problem. As shown in Figure 5.16, the SP-14

has an uncharacterized actuation region of about 4 ms, which may include the dead-time and the highly non-linear region immediately following it. The actual amount of fuel delivered during a pulse less than 3 ms wide was assumed to be significantly subject to manufacture tolerance and other conditions besides the injection pulse-width. With a prescribed 30 psi fuel pressure, the injection pulse-width for stoichiometric operation at idle is about 3 ms, which falls right into the uncontrollable region of the injector.

Secondly, the idle operation itself is semi closed-loop. To get better overall fuel economy and emissions, the PCM marginally regulates the idle speed (through the idle air control) to its lower limit. The engine operates on the verge of instability as indicated by frequent change of operating point. More delicate control and efficient learning under frequent RPM fluctuations are needed.

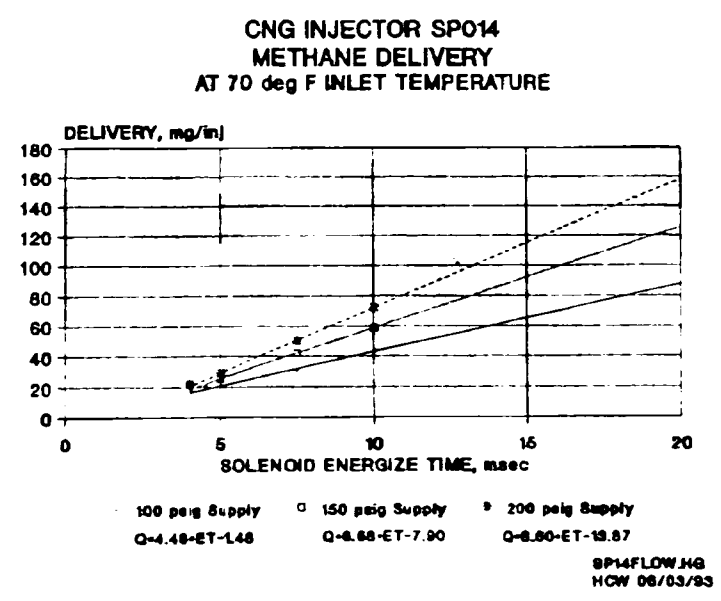

Figure 5.16 SP014 CNG Injector Characteristics [20]

Two major modifications were made to improve the idle operation. Both of them target the frequent operating point shifts at idle, and have little effect on steady-state mid/high RPM operation, during which the engine stays at one operating point for extended period of time.

The first modification was to change absolute control to incremental control of the injection pulse-width. In the absolute control mode, the injection command INJPW is the direct output of the PI control u(k). The PI integrator initial value u(0) is reset to the stored table value only when a fast transient is detected. The shift of operating point, which happens frequently during the idle, will not reset it. In the presence of these frequent operating point shifts at idle, slow PI control alone could not keep up and induce speed fluctuations. In the incremental control mode, the PI integrator is reset to zero upon the detection of a fast transient. The injection command INJPW is the sum of u(k) and the stored table value corresponding to the current operating point. Table lookup takes place in every calculation of the control output, which makes the incremental control more open-loop and responsive in the presence of frequent operating point shifts

The second modification was intended to improve the associative capability of the learning control. The original learning control only updates the single table element that corresponds to the current operating point. This method becomes inefficient when the engine stays at an operating point for only very short time, during which an effective learning may not yet well in place. The noise in the learning process often causes the overall effect of these short training sessions close to zero. The solution is to increase the associativeness of the learning, with which not only that single table element corresponding to the current operating point is adapted, but also those elements surrounding it. Among other available techniques, neural network, with its good mapping and generalization capabilities, seem to be promising. A cerebellar model articulation controller (CMAC) neural network for engine air/fuel ratio control has been reported in

the literature [5]. There are also some disadvantages associated with neural network techniques. Among these advantages are large computation amount and/or high memory requirement, which are undesirable for an embedded controller. Again due to the time constraint, a simple associative learning was used instead.

Every time a table element F(i, j) is updated using W(k), its four surrounding elements are adapted as follows. The coefficient β, which determines the associativeness of the learning, was set at 0.125 during the experiment.

$$
\begin{aligned}
&F(i, j) = F(i,j) + W(k);\\
&F(i-1, j) = (1-\beta)F(i-1, j) + \beta\,[F(i-2, j) + F(i, j)]/2;\\
&F(i+1, j) = (1-\beta)F(i+1, j) + \beta\,[F(i+2, j) + F(i, j)]/2;\\
&F(i, j-1) = (1-\beta)F(i, j-1) + \beta\,[F(i, j-2) + F(i, j)]/2;\\
&F(i, j+1) = (1-\beta)F(i, j+1) + \beta\,[F(i, j+2) + F(i, j)]/2. \qquad (5.5)
\end{aligned}
$$

5.2.4.3 Software Implementation

The whole algorithm was implemented in two subroutines. An event-based subroutine (CRKC) implements the PI control and W(k) calculation, while another time-base subroutine (CTLINT) implements the anticipatory feed-forward control and the learning control. Two subroutines communicate via a group of access-controlled global variables.

The MAP sensor output, which, at high RPM, is superimposed with observable fluctuation with a period of 1/6 of an engine cycle, is event-based sampled and filtered every 60° of crank- angle. The readiness of the O_2S sensor is checked before engaging the closed-loop control as well as throughout the closed-loop operation.

A state machine governs the transition between closed-loop and open-loop operations. The state machine, along with the simplified flow charts of the two subroutines, are shown in Figure 5.17.

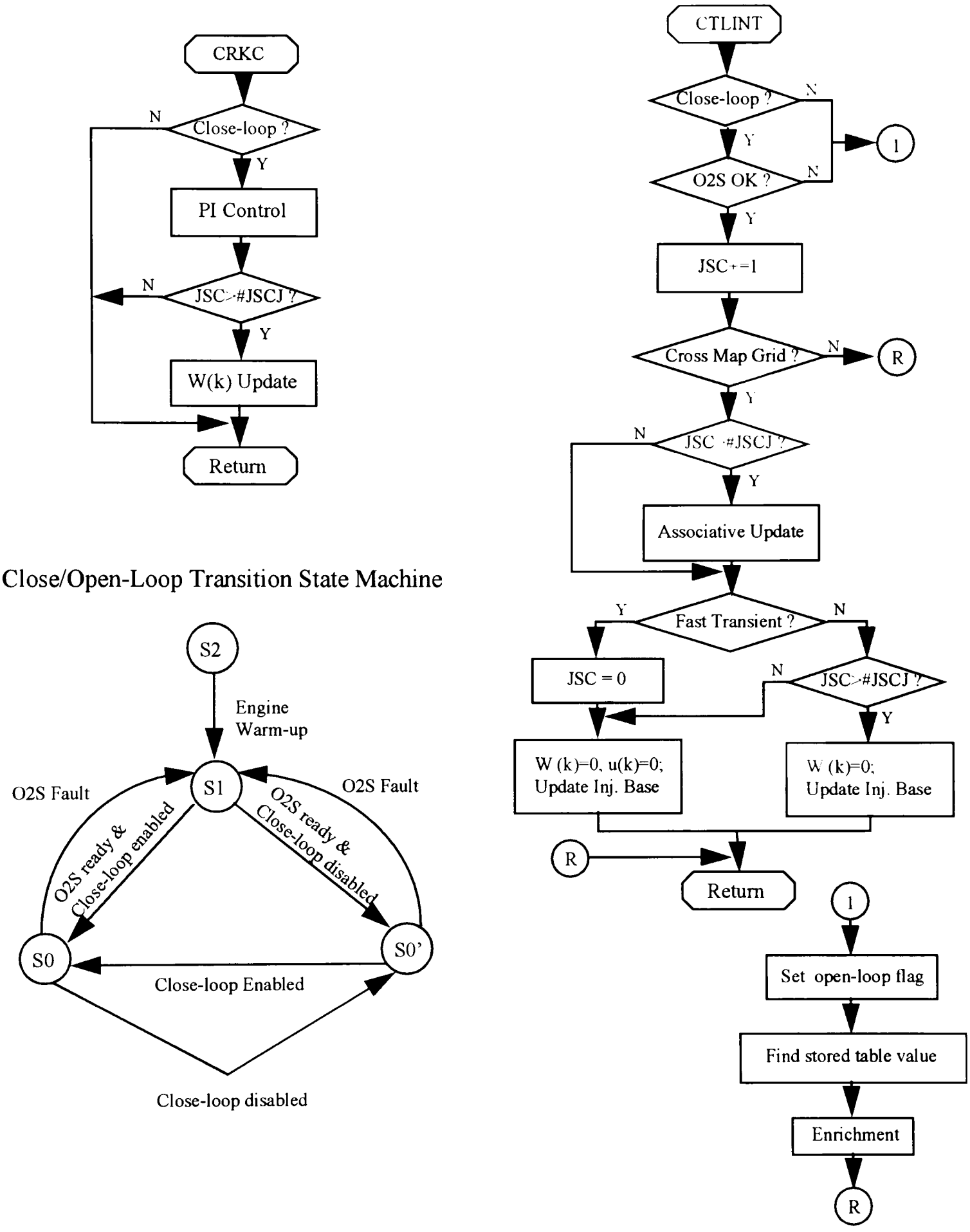

Figure 5.17 Closed-loop Learning Control Flow Chart

5.2.4.4 Experimental Result

Extensive experiments were conducted to test the software, during which many modifications were made to improve its control performance. The experimental results to be presented here were actually taken after the engine switched back to the Bosch CNG injectors. As had been expected, the performance of the TTUCM improved significantly with these smaller injectors. Idle speed fluctuation reduced to negligible. Learning and closed-loop control became much more stable and effective.

The engine system was setup as follows: Bosch CNG injectors, 80 psi fuel vapor pressure, O_2S sensor connected to both PCM and TTUCM, EGR disconnected, PCM injector control outputs connected to dummy injector load. No other relevant indication of error than the EGR malfunction was given by the PCM.

The engine ran stablely in open-loop before it warmed up and the O_2S sensor got ready, upon which the closed-loop learning control was engaged. Most experiments were done while the engine was at idle, which was thought to be the most difficult operating mode as far as closed-loop steady-state air/fuel ratio control was concerned. The modifications discussed in the last section significantly improved the idle operation without adversely affecting the high RPM end performance. All the results given below were obtained with the final control software.

The initial fuel map was deliberately enriched to insure a smooth open-loop operation right after start-up. After the engine got into closed-loop, the fuel map was adapted for the stoichiometric operation by the learning control. Figure 5.18 shows the partially adapted fuel map recorded ten minutes into the closed-loop operation. During

these ten minutes, the Minivan was driven on the chassis dynamometer while the TTUCM was trained. The adapted map region covers full RPM range at light load. Comparing Figure 5.18 with the initial fuel map shown in Figure 5.12, it can be seen that the associative learning generated smooth adaptation of the fuel map.

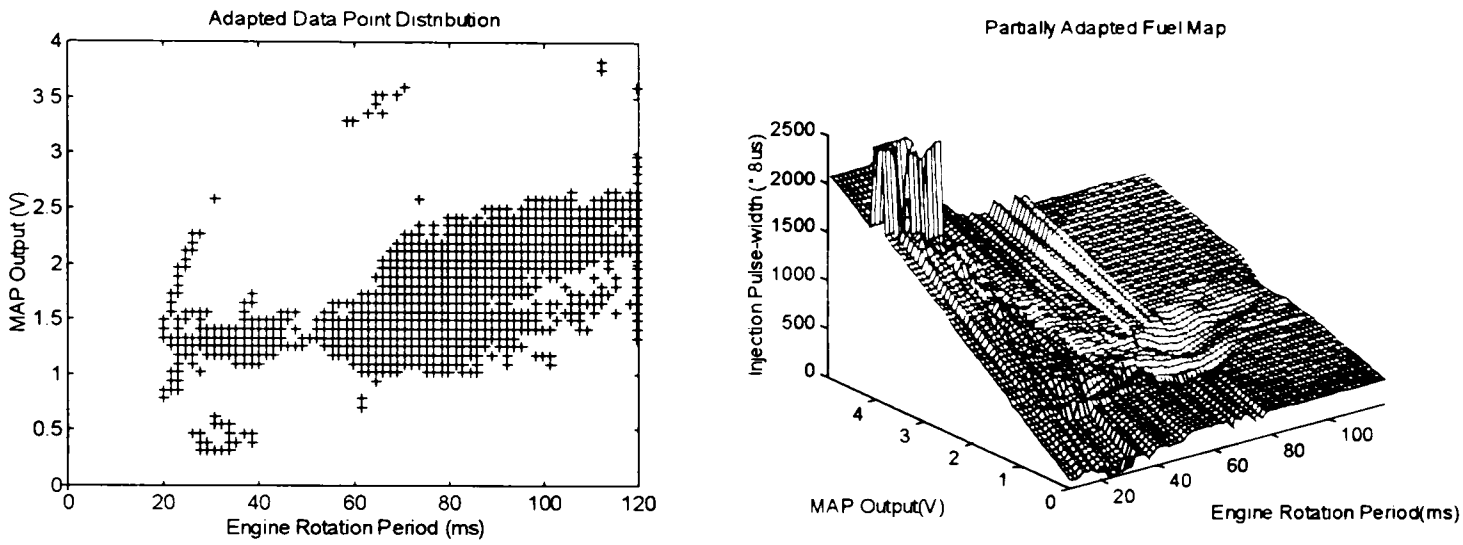

Figure 5.18 Partially Adapted Fuel map

The closed-loop control induces oscillations in the output of O_2S sensor. The oscillation frequency, which varies with the engine speed, is an indication of the closed-loop control performance. Faster oscillations indicate a more responsive closed-loop control. Figure 5.19 and 5.20 show the outputs of the O_2S sensor under the TTUCM control and PCM control, when the engine is at idle and 3000 RPM (no load), respectively. The performance of the TTUCM is seen to be comparable to that of the PCM at idle. At 3000 RPM, the TTUCM seems to be less responsive, which can be improved with the introduction of gain-schedule PI control. In both experiments, the PCM seemed to run the engine a little too rich.

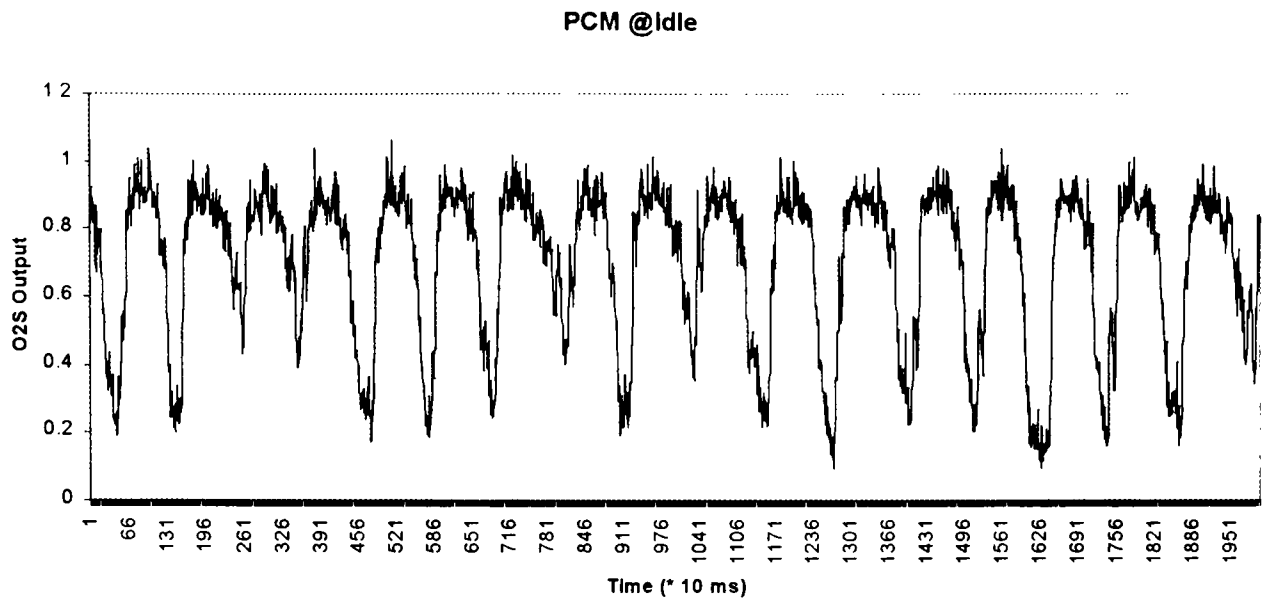

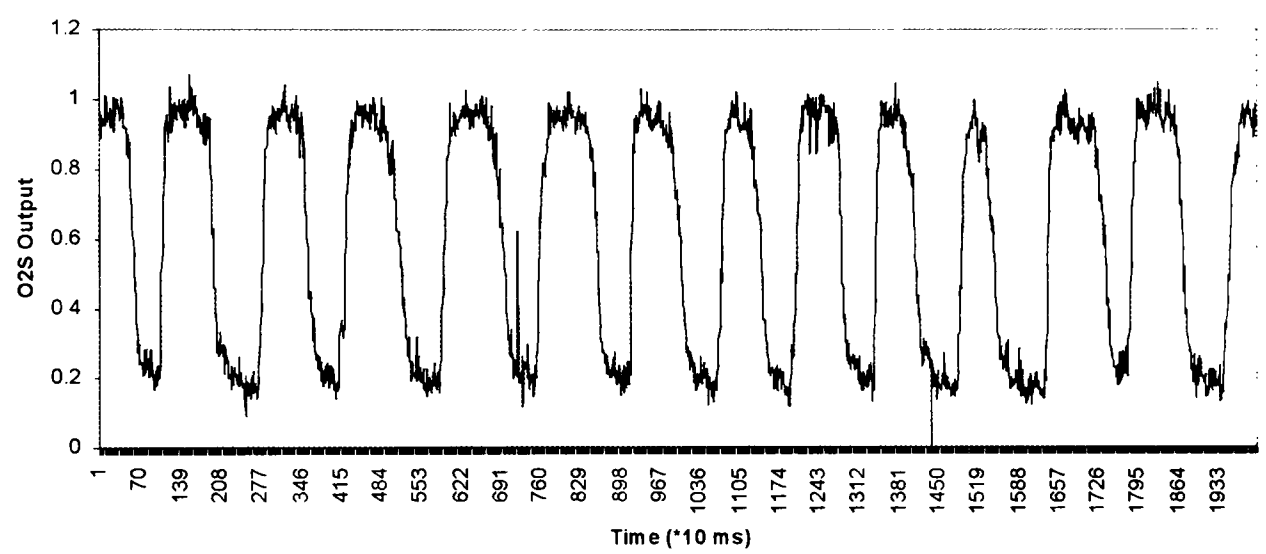

Figure 5.19 TTUCM and PCM Control at Idle

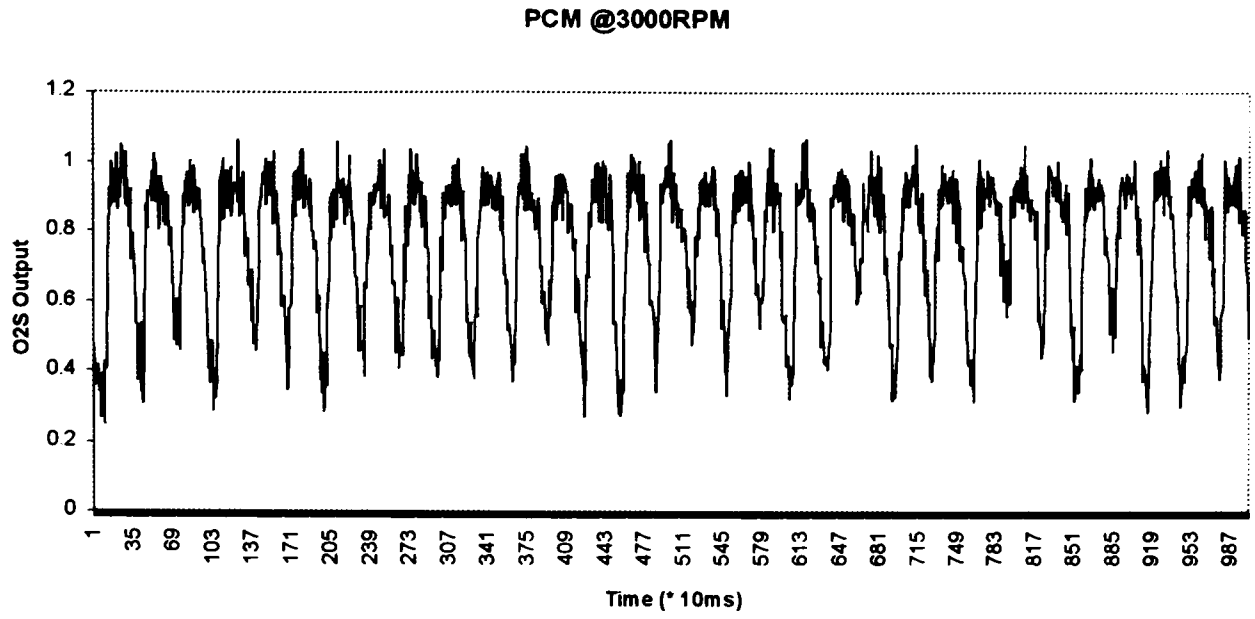

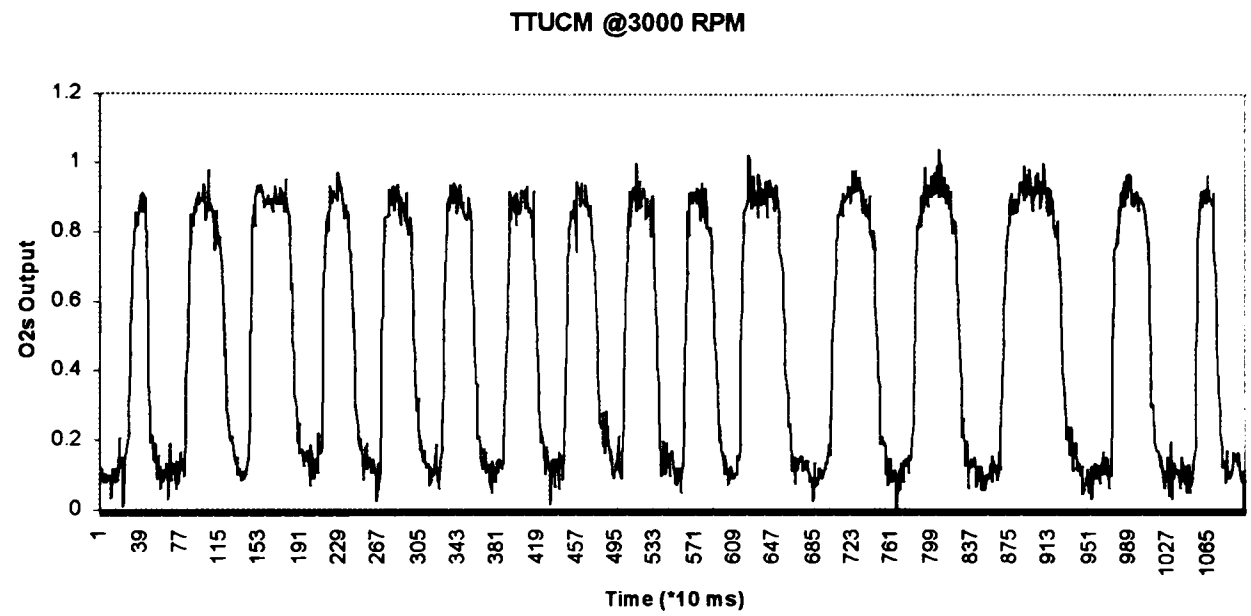

Figure 5.20 TTUCM and PCM Control at 3000 RPM (no load)

Engine tailpipe emissions at idle are compared in Table 5.2 between the PCM control and the TTUCM control. The reading was taken from the ECOM gas analyzer. The unit ppm stands for parts per million.

Table 5.2 Comparison of Engine Emissions

	CO (ppm)	NO (ppm)	NO2 (ppm)	NOx (ppm)	Lambda	Efficiency
TTUCM	5	2	0	2	1.01	89.1%
PCM	8	1	0	1	1.00	87.9%

The experimental results prove that the current version of the TTUCM control software can accurately control the steady-state air/fuel ratio to obtain low emissions, while maintaining a smooth operation. The learning control effectively compensates for the errors in the initial control data.

CHAPTER 6

CONCLUSIONS AND FUTURE WORK

A microprocessor-based engine controller has been preliminarily developed in this thesis, from hardware to software, from theory to implementation. This work makes the first step in the long range research effort to develop an engine controller whose design is completely known and accessible to us, and can thus be fully optimized for any specific alternative fuel engine system.

The controller hardware has been designed and built with good flexibility and configurability. Software has been developed to control the engine air/fuel ratio in closed-loop, and the operation of the converted engine fuel system. Learning capability is built into the software to facilitate the engine calibration as well as to make the system more adaptive and robust.

The current development proves the feasibility of designing such an engine controller, but also indicates that a lot more work has to been done to develop it into a robust full-featured engine controller.

First, the engine idle operation still needs to be improved. A high flow rate injector with smaller dead-time and non-linear region will be very helpful. Map grid size and the coordination of the closed-loop control with the anticipatory feed-forward control are to be more closely studied, with emphasis on their effects on system stability.

Second, dynamic compensations should be introduced in the air/fuel ratio control after the TTUCM is able to control the engine to operate stablely in closed-loop under all

operating conditions. More accurate engine physical model may be needed before the design of dynamic compensations.

Third, a UEGO can be incorporated into the system to allow for the applications of many advanced control techniques, which have the potential of more accurately controlling the air/fuel ratio and engine operations.

REFERENCES

[1] King, Robert D.; Haefner, Kenneth B.; Salasoo, Lembit; and Koegl, Rudolph A. "Hybrid Electric Transit Bus," IEEE Spectrum, July 1995, pp.26-31.

[2] Maxwell, Timothy T.; and Jones, Jesse C. Alternative Feuls: Emission, Economics, and Performance, SAE Inc., Warrendale, PA, 1995, pp. 3-4, 9-10, 37-38,

[3] Stone, Richard. Internal Combustion Engines, 2nd Ed., SAE Inc., Warrendale, PA, 1994, pp. 1-2, 175, 122, 124, 148

[4] Jurgen, Ronald. Automotive Electronics Handbook, McGraw-Hill, New York, 1995, pp. 1.4, 6.17, 12.2-12.3, 12.6,

[5] Shiraishi, Hitoshi; Ipri, Susan L.; and Cho, Dong-il D. "CMAC Neural Network Controller for Fuel-Injection Systems," IEEE Transactions on control systems technology, vol. 3, No.1, March,1995.

[6] Chrysler Corporation, Service Manual: 1995 Chrysler Town and Country Minivan, Detroit, MI, 1995, pp. 8D-5, 14-27, 14-35, 14-40, 14-41

[7] Motorola Inc., User's Manual: MC68F333, Phoenix, AZ, 1994, pp. 1.1-1.4, 3.1, 3-66, 4.1, 5.1-5.5, 10.1

[8] Motorola Inc., Reference Manual: M68300 Family CPU32, Phoenix, AZ, 1990, pp. 1.1-1.2

[9] Motorola Inc., Reference Manual: Modular Microcontroller Family ADC, Phoenix, AZ, 1993, pp. 1.1.

[10] Motorola Inc., Reference Manual: M68300 Family TPU, Phoenix, AZ, 1990, pp. 1.1-1.5, 3.13, 3.22, 3.73, 3.85, 3.113.

[11] Motorola Inc., User's Manual: M68MPFB1632, Phoenix, AZ, 1994, pp. 1.1-1.3, 3.1

[12] Datel Inc., Data Sheet: TWR-5/3000-12/500-D12, Boston, MA, 1995.

[13] Philips Semiconductors, Product Specification: BUK856-400IZ, Sunnyvale, CA, 1993.

[14] National Semiconductor, Data Sheet: LF441 Low Power JFET Input Op-amp, Sunnyvale, CA, 1990.

[15] Fekete, N. P., Powell, J. D., et al. "Model-Based Air-Fuel Ratio Control of a Lean Multi-Cylinder Engine," SAE 950846, 1995

[16] Hendricks, Elbert; and Sorenson, Spencer C. "Mean Value Modelling of Spark Ignition Engines," SAE 900616, 1990.

[17] Chang, Chen-Fang; Fekete, Nicholas P., and Powell, J.David. "Engine Air-Fuel Ratio Control Using an Event-Based Observer," SAE 930766, 1993

[18] Nakaniwa, S., Furuya, J. and Tomisawa, N. "Development of nest-structured learning control system," SAE 910084, 1991

[19] Ishii, J., Kurihara, N., et al. "An automatic parameter matching for engine fuel injection control," SAE 920239, 1992

[20] BKM SP014 CNG Injector Data Sheet, Clean Air Partners, San Diego, CA, 1997

[21] 1998 FutureCar Challenge: A Student Engineering Design Competition Proposal. College of Engineering , Texas Tech University.

[22] Hendricks, Elbert; Jensen, Michael; Kaidantzis, Patrick et al. "Transient A/F Ratio Errors in Conventional SI Engine Controllers," SAE 930856, 1993.

[23] Turin, Raymond C.; and Geering, Hans P. "Model-based Adaptive Fuel Control in an SI Engine," SAE 940374, 1994

APPENDIX

TTUCM CONTROLLER HARDWARE

This appendix contains information on TTUCM controller hardware assembly

Pertinent notes are included in the pages preceding the schematics, layouts and tables.

A.1 Interface Board Schematics

The following three pages contain the schematics for the interface board. For each type of interface, schematics are given for only one of multiple identical channels available on the interface board. The shorthands in the parentheses above each circuit are the names of interface types used in PCB layout annotation., and following are the numbers of channels available on the interface board.

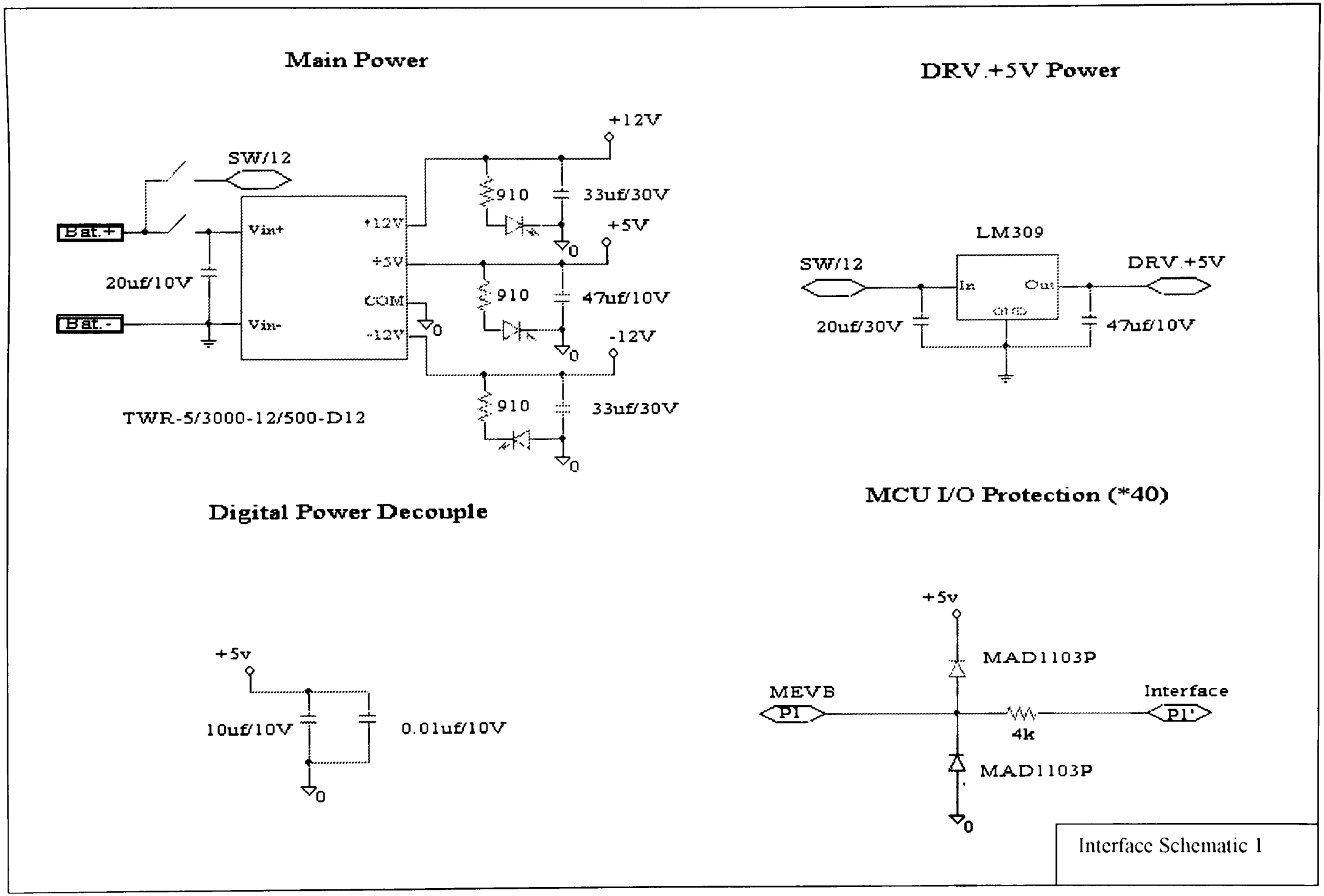

Figure A.1 Interface Board Schematics 1

Universal Isolation Driver (DR*16)

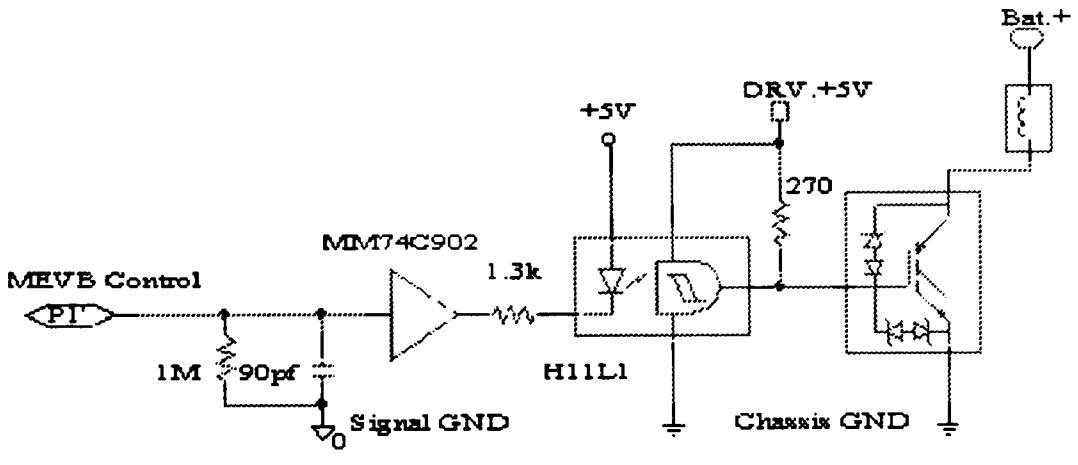

Isolation Digital Input (ID*6)

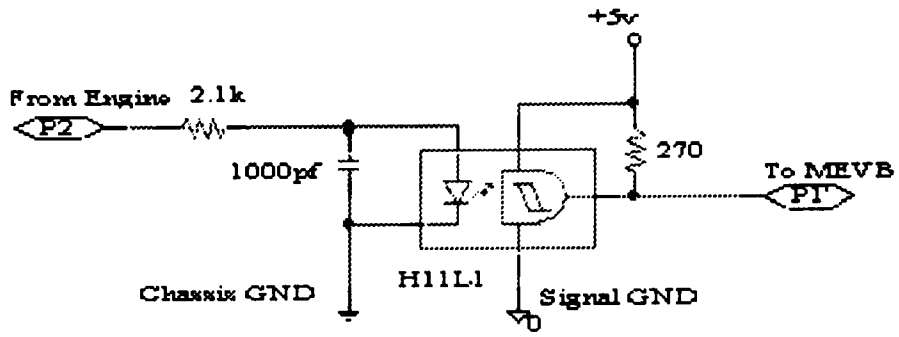

General Analog Interface (AD*8)

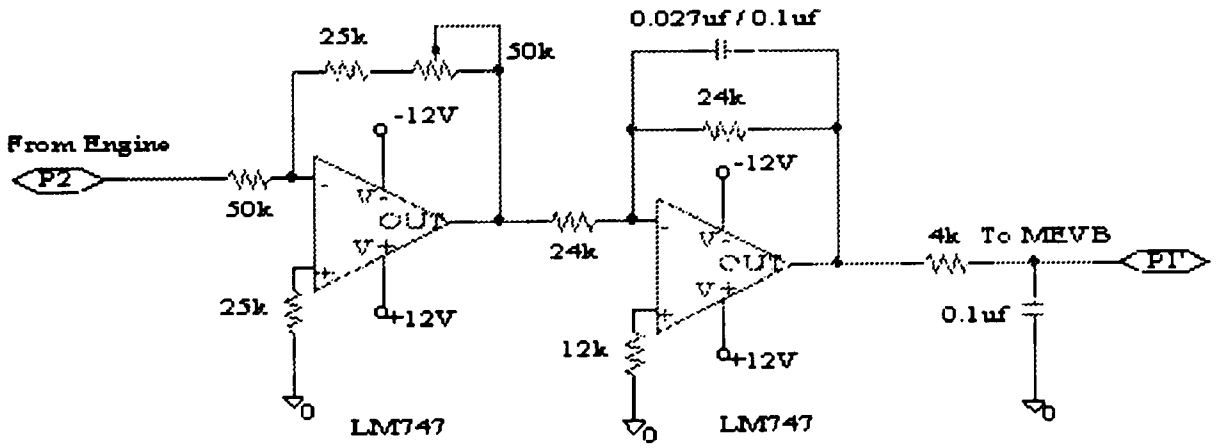

Direct Digital Input (DD*3)

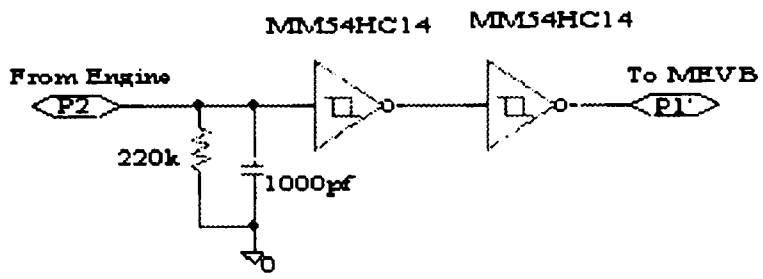

Interface Schematic 2

A.2 Interface Board Schematics 2

A.2 Interface PCB Layout

Given in the next three pages are the interface PCB layouts on component side, solder side and silkscreen layer. They are not in their actual sizes. In the silkscreen layout, all the interface channels are named. The name is placed close to the major component of the channel, and is used to refer to that channel in Table A.1. Some corrections and modifications were made after the PCB was manufactured. They are indicated in the layouts and listed below.

(1) Jump-wire between two pins.

(2) Cut the trace.

(3) Cut the trace.

(4) Jump wire to (3).

(5) Jump wire to (6).

(6) Jump wire to (5).

(7) Flip the symbol horizontally.

Something is wrong with these printouts. Three solder pads of each IGBT should not be connected together. However, the original print and the PCB are correct.

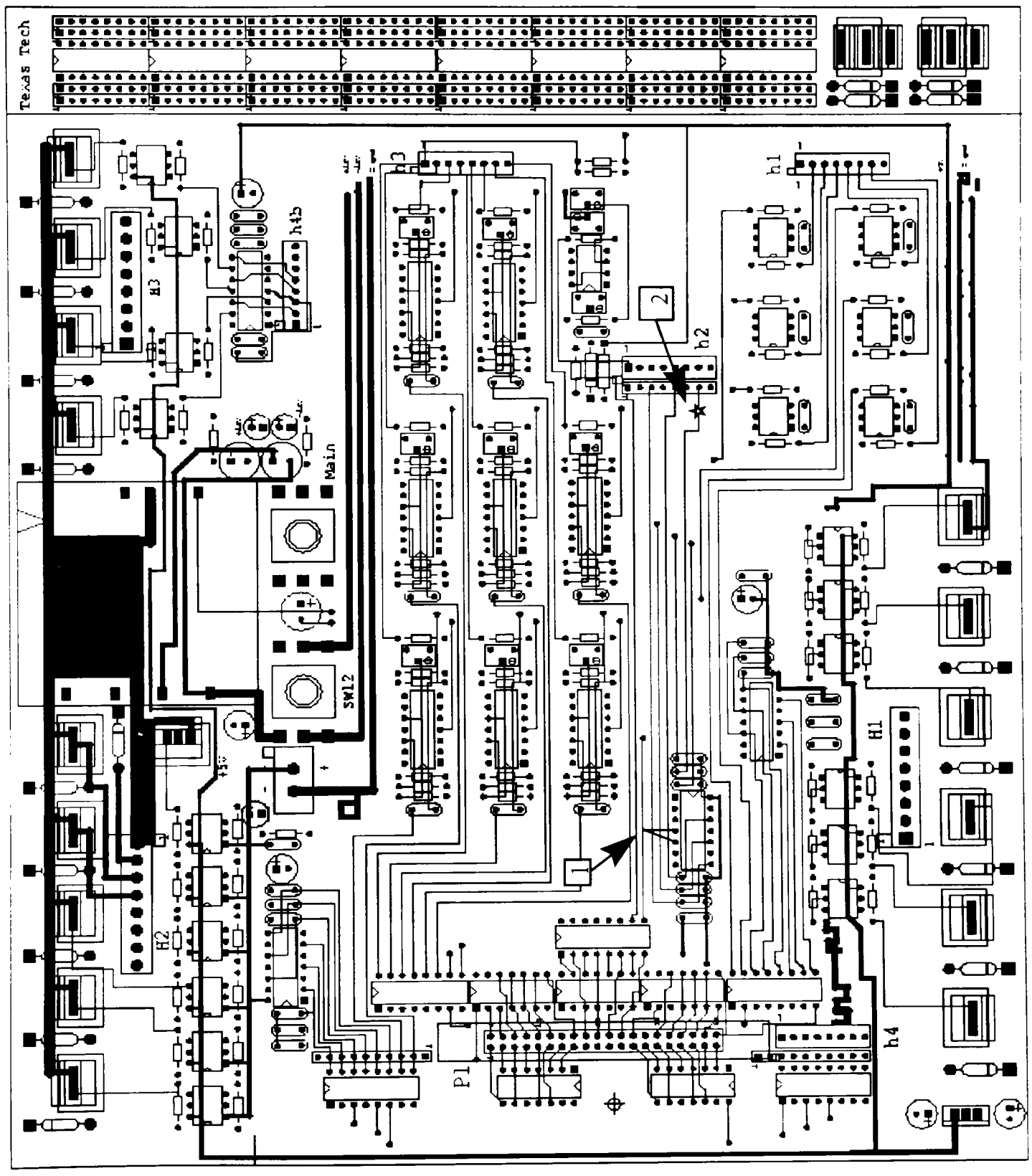

Figure A 3 Interface PCB Layout (Component Side)

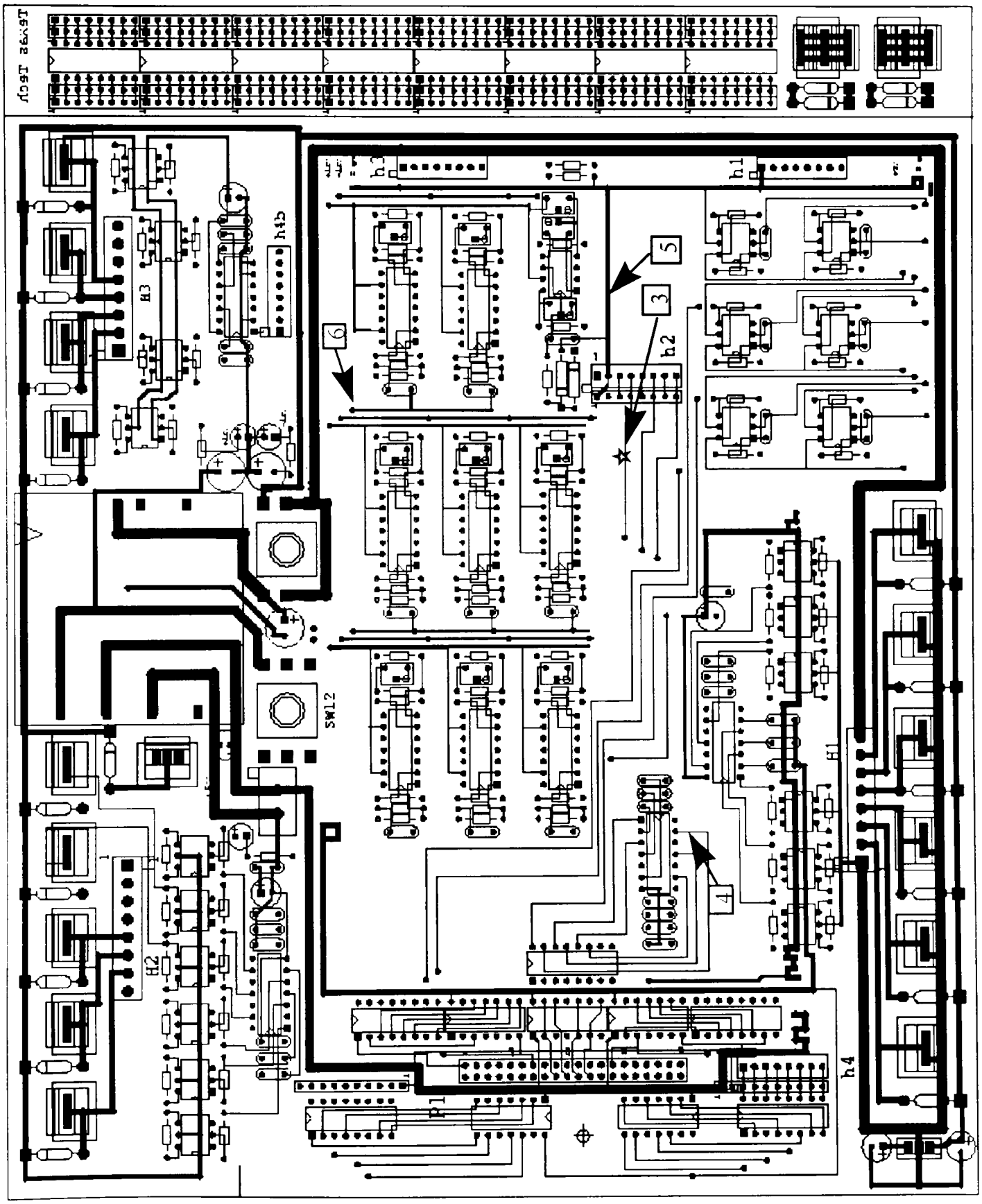

Figure A-4 Interface PCB (Solder Side)

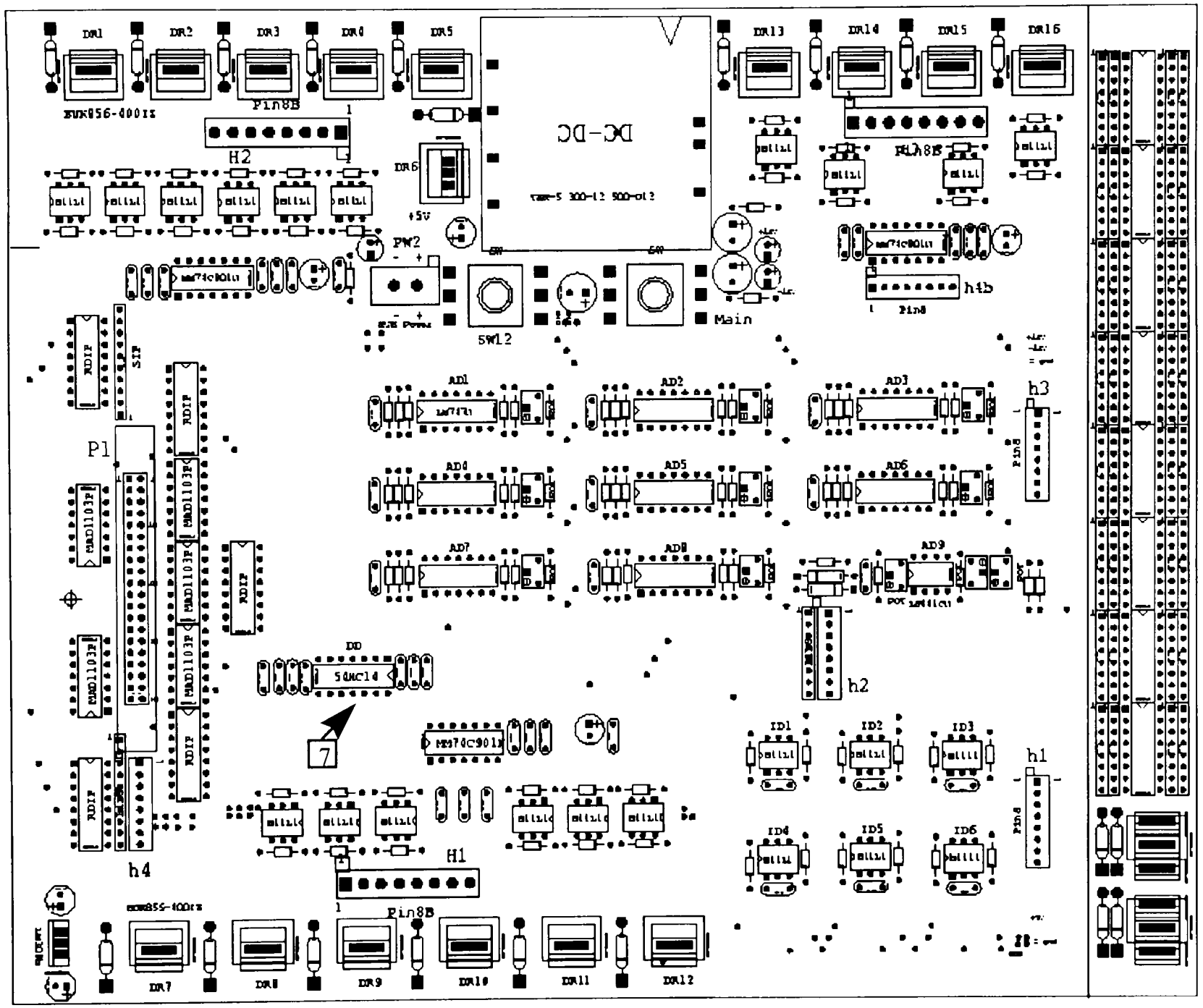

Figure A.5 Interface PCB (Silksreeen)

A.3 Interface Connection

Connectors are extensively used in the TTUCM assembly to obtain channel assignment flexibility as well as easy detachment and replacement of components. Table A.1 gives the signal definitions of all the connector pins. The flow of signals can be followed by referring to Table A.1, which is explained in the following example.

Find the MAP in the column "Engine Signal" Then in column "Engine End Connector" we see it is connected to the 30th pin of P2 connector -- P2 (30). Moving down the row, it goes through h3 (7) to channel AD7, and then is output to P1(10) where it exits the interface board and enters the MEVB.

The above signal flow applies to engine sensor/switch signals. Actuator control signals flow in the opposite direction: P1 $\rightarrow$... $\rightarrow$ P2.

The MEVB I/O assignment is given in Table A.2. The connections were made using wire-wrap and are alterable.

Table A.1 Interface Connection

	MCU End Connector[1]	Interface No.[2]	Engine End Sub Connector[3]	Engine End Connector[4]	Engine Signal[5]
Driver Group I	P1(1, 3, 5, 7, 9, 11)	DR1-DR6	H2(7, 6, 5, 4, 3, 2)	P2(33, 15, 34, 16, 35, 17)	(NC, MF, T/B, HP, Tinj2, ECTB)[6]
Driver Group II	P1(30, 32, 34, 36, 38, 40)	DR12-DR7	H1(7, 6, 5, 4, 3, 2)	P2(1, 20, 2, 21, 3, 22)	Inj(6-1)[7]
Driver Group III	P1(27, 29, 31, 33)	DR13-DR16	H3(2, 3, 4, 5)	P2(18, 19, 36, 37)	(Tinj1, Ign(1-3))[8]
A/D Group I	P1(13, 15, 2, 4, 6, 8, 10, 12)	AD1-AD8	h3(1-8)	P2(NC, 13, 32, 12, 31, 11, 30, 29)	(Bat.Volt, FPT1, Knock, TPS, FPT2, ECT, MAP, NC)[9]
A/D Group II	P1(23)	AD9	h2(1)	P2(10)	Upstream O2
Direct Dig.Input Group	P1(22, 20, 18, NC, 21, 19)	DD	h2(3, 4, 5, 6, 7, 8)	P2(NC, 28/2, 28/1, 8/1, 8/2, 27)[11]	(-, -, CRK, CAM, -, NC)[10]
Isolation Dig.Input Group	P1(14, 16, 17, 24, 26, 28)	ID3-ID, ID6-ID4	h1(2, 3, 4, 5, 6, 7)	P2(7, 26, 6, 25, 5, 24)	(Stop lamp, ASD, Ign SW, P/N SW, Torque req, NC)[12]

26 CAM

Note:

1 P1 is the 40-pin header connector on the interface board, connected to the MEVB.

2 The actual locations of the interface channels are shown in Figure A.6.

3 Connectors (various types) that connect the signals in a group to the P2.

4 P2 -- the 36-pin male D-sub connector mounted on the side of box.

5 These engine signals have been connected to P2.

6 Also connected: H2(1) → P2(14) → GND, H2(8) → NC (not connected). Signal full name: MF-- Main Fuel Control Relay, T/B -- Fuel Tank Top/Bottom Control Relay, HP -- High Pressure Control Relay, Tinj2 -- Throttle Injector 2, ECTB -- ECT Bias Control Relay.

7 Also connected: H1(1) → P2(23) → GND, H1(8) → P2(4) → Bat.+

8 Also connected: P1(25, 27, 29, 31, 33, 35, 37, 39) → h4(1-8) → h4b(1-8). Signal full name: Tinj1 -- Throttle injector 1.

9 h3(1) has been connected to the battery positive on the interface board (for battery voltage measurement). Signal full name: FPT -- Fuel Pressure Transducer.

Table A.1 Continued.

[10] Also connected: h2(2) → P2(9) → S.GND.

[11] The underlined items are actually not connected. Signal flow: CRK → P2(28) → h2(5) → 2*DD → P1(18).

[12] Not included: h1(1) → S.GND → NC, h1(8) → NC.

Table A.2 MEVB I/O Assignment

MCU I/O	Engine Signal
TPU0	Crankshaft Position
TPU1	Crankshaft Position
TCR2	Crankshaft Position
TPU2	Camshaft Position
TPU3 - 8	Injector 1 - 6
AN0	MAP
AN1	ECT
AN2	EGO
AN3	TPS

A.4 Relay Submodule Schematics

The schematic for the relay submodule is given in the next page.

Relay #1

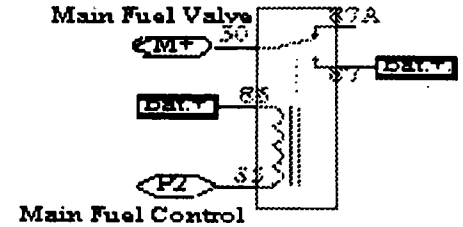

Relay #2

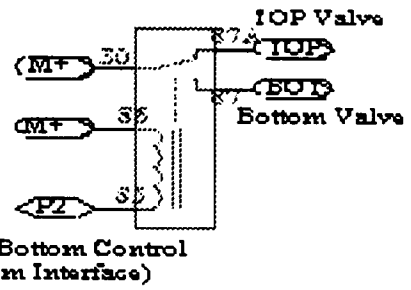

Relay Box Connectors
(Look into the box)

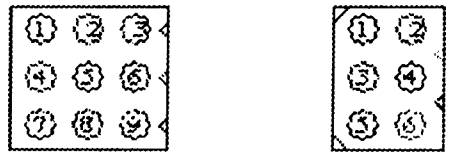

1-- +12
2-- ECI
3-- Iop Valve
4-- Bottom Valve
5-- High Pres. Valve
6-- Main Fuel Vavle
7-- GND

1-- ECI Bias Control
2-- Iop/Bottom Control
3-- High Pres. control
4-- Main Fuel Control

Relay #3

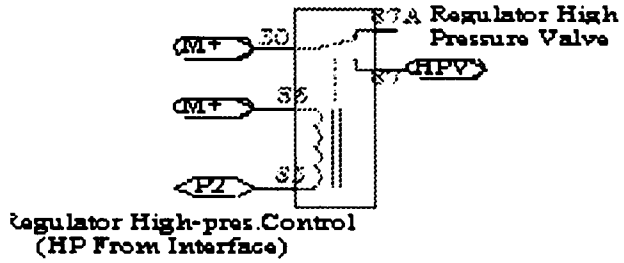

Relay #4

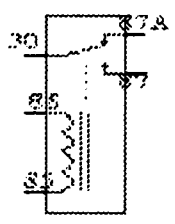

In-box DIN10 Connector

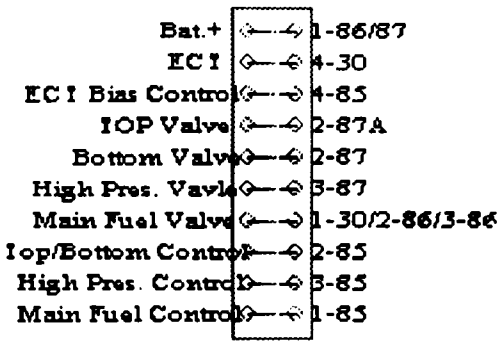

Relay Submodule

A.6 Relay Submodule Schematics

PERMISSION TO COPY

In presenting this thesis in partial fulfillment of the requirements for a master's degree at Texas Tech University or Texas Tech University Health Sciences Center, I agree that the Library and my major department shall make it freely available for research purposes. Permission to copy this thesis for scholarly purposes may be granted by the Director of the Library or my major professor. It is understood that any copying or publication of this thesis for financial gain shall not be allowed without my further written permission and that any user may be liable for copyright infringement.

Agree (Permission is granted.)

Student's Signature — Date

Disagree (Permission is not granted.)

Student's Signature — Date